

UCSF

UC San Francisco Electronic Theses and Dissertations

Title

CRISPR screen in regulatory T cells reveals modulators of Foxp3

Permalink

<https://escholarship.org/uc/item/8r68w2ms>

Author

Cortez, Jessica T

Publication Date

2020

Supplemental Material

<https://escholarship.org/uc/item/8r68w2ms#supplemental>

Peer reviewed|Thesis/dissertation

CRISPR screen in regulatory T cells reveals modulators of Foxp3

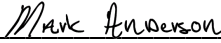
by
Jessica Cortez

DISSERTATION
Submitted in partial satisfaction of the requirements for degree of
DOCTOR OF PHILOSOPHY

in
Biomedical Sciences


in the
GRADUATE DIVISION
of the
UNIVERSITY OF CALIFORNIA, SAN FRANCISCO

Approved:

DocuSigned by:

657D61B3C699406... Mark Anderson
Chair

DocuSigned by:

K. Mark Ansel

DocuSigned by:

7F25CDCE383C4A8... Alexander Marson

Committee Members

Copyright 2020

by

Jessica T. Cortez

To my mother, Annette, who has always been my guiding light.

To my father, Joe, who never forgets to remind me how proud he is of me.

I am eternally grateful for your unconditional love and support.

Acknowledgements

First and foremost, thank you to Alex for his all of his mentorship and support. My respect and admiration for your ability to think, communicate and lead has only grown over time as you have continuously demonstrated what it is to be a thoughtful, collaborative and detail-oriented scientist. You have an incredible ability to distill and clarify information, which has not only been invaluable during my training but has helped the lab's work gain visibility across a variety of platforms. It's been really motivating to be a part of a team with widespread recognition of our efforts. I've also really valued your frequent expressions of appreciation to the lab for the work that we do including the multiple pep talks you have given me personally through the years that helped lift me up when I was feeling discouraged and helped me forge ahead to the finish line. Thank you Alex, I'm so grateful to have had your help and encouragement throughout this process.

Mark Anderson, I'm so thankful for the opportunity you gave me to come train in your lab as an undergraduate over the summer and as a technician which helped lay the foundation of my scientific training. It's been so amazing to be able to continue having you as a mentor throughout grad school as the chair of my thesis committee. Thank you for always believing in me especially when I struggled to believe in myself. Mark Ansel, thank you for your great advice and suggestions during my committee meetings and for including me on multiple outreach trips which have been super fun and rewarding to be a part of. I feel so lucky to have been part of a program with a director that cares so deeply about the students and always makes us feel heard.

Thank you to all members of the Marson lab, past and present, who have contributed to my training in invaluable ways and provided great role models and friendships throughout my grad schools years and beyond. Thank you all for making the lab such a great environment to work in that is incredibly supportive and fun. I truly feel so grateful to be surrounded by a group of such thoughtful, smart and funny scientists.

Specifically, thank you to Eric Shifrut who was instrumental in helping me develop the screening pipeline. Eric dedicated many hours to help me analyze data and teach me how to code in R and I am endlessly grateful for his guidance, time and company. Thank you to Oren Shaked, my science teammate, for being willing to work together on a challenging project and learning with me along the way; it was so much fun. Thank you to my fellow grad students – Joe, Theo, Dimitre, Cody and Jenny – I will always cherish our grad student drink ups and all of your supportive talks. Dimitre, our talks in particular have helped me through some challenging times and I truly appreciate all of your encouragement and advice. Michelle, David and Youjin - you have all contributed to my training in a really meaningful way and I'm so grateful for all the time you all took to help train and support me. Kathrin, Michael and Brian, my Treg buddies - thank you for always being willing to share reagents and knowledge. Murad, thank you for your daily banter, your advice on even the most insignificant of things (being as you were usually the closet person to me) and your friendship. Sagar, thank you for always being willing to help out and keeping things amusing by filling every exchange with rampant sarcasm. Ruby, Ujjwal, Franzi, Dan - I always enjoy my talks with you guys, thank you for keeping the lab

a fun place to work. Edward, Tori, Ralf and Zach – I've really enjoyed working with you all for the short time we could, and I'm excited to see how your projects unfold.

Thank you to all of our amazing technicians, especially Zhongmei - for working so incredibly hard and being super skilled at what you do. Jon – for taking care of all the little things that keep the lab functioning smoothly and for always being down to play some games. Victoria, Ryan, and Shane – for helping me organize blood draws and deliveries. Thank you to Amy, Caroline, Ian and Sid, who have helped me with various experiments or analyses. Thank you to Devin for being an incredible friend and helping me pull off an amazing charity bake sale.

Thank you to all of the additional mentors I've had during my time at UCSF. Thank you to Jeff Bluestone for all of your mentorship and advice that helped overcome significant scientific challenges and helped shape my story. Thank you to Frederic Van Gool, for your support, technical expertise and always stopping to chat. I'm so excited to continue working with you both at Sonoma. Thank you to Mike Waterfield, for taking me on as a summer student, encouraging me and being incredibly patient with me when I made mistakes – having an excellent mentor like you early on made it possible for me to imagine continuing down the path to grad school. Thank you to Jimmie Ye and Luke Gilbert for serving on my quals committee. Thank you to my rotation mentors Max Krummel, Mark Headley, Trevor Burt and Joanna Halkias and journal club coaches Qizhi Tang and Mike Rosenblum for your investment in my training.

Thank you to Maria Mouchess and Tangsheng Yi, who mentored me during my summer internship and Genentech. Thank you to all of the administrative staff that works behind the scenes to make sure everything goes to plan – especially Demian Sainz, Jennifer Okano, Melanie Gordon, Ned Molyneaux, Lily Yu, Monique Piazza and Jonathon Wilson. Thank you to the incredible flow core who has made sorting and analysis as painless as possible with their superb assistance – and especially Vinh Nguyen who has not only helped me in the flow core at all hours of the day or night, but has selflessly helped me with islet preps and pancreatic LN dissections as well, and is an incredible asset to the entire UCSF research team.

Thank you to the amazing leadership team of ImmunoXX, it's been such a pleasure to be part of this group and I'm so proud of each and every one of you and everything we have accomplished. Thank you to Grace Prator, for the opportunity to refine my mentoring skills and for being steadfast in her dedication to science.

Thank you to the entire BMS community and all of my classmates. I am so thankful to have had such a wonderful, fun and supportive group to be a part of during grad school. Thank you to my grad student support group, my closest cohort buddies – Casey, Dan, Rebecca, Carlos and Ariane - who regardless of shelter in place still meet with me weekly over Zoom so we can drink wine and vent. They have been the people I have turned to during moments of stress and panic and I so appreciate their listening ears and reassuring praises. Especially thank you to Ariane, who has been my teaching partner for 4 years for SEP. We've taught kids about bacteria, DNA and squid anatomy and it's always so

much fun and a breath of fresh air getting out of the lab for outreach. At the end of the year we always get thank you letters from the kids which is always so rewarding and cute.

Thank you to my therapist, Jeanne Stanford, for getting me through the most difficult tragedy I have ever personally experienced, in the middle of graduate school. I'm so thankful to UCSF for prioritizing their student's mental health and allowing me to access her counseling services.

Thank you to my incredible friends – Malika, Tyler, Frankie, Jeremy, Shannan, Brittany, Suzanna, Aryana, Christine, Akila and Wana - for preserving my work-life balance and always lending an ear, you guys have all been an amazing support system and I'm so thankful to have all of you in my life. Thank you to my family – Destiny, Rosemary, Alexis, for your love and support. Thank you to my sister Jodie, for always being down for an adventure and sticking up for what you believe in, but mostly for making me so proud to be your sister. Thank you to my dad who has been calling me Dr. Jessica since I started grad school and never forgets to tell me how proud he is of me. Thank you for being my biggest fan. I want to express eternal gratitude to my mom, who has instilled in me the value of not stressing over the things I cannot control, to do the best I can and to focus my energy on the things that truly matter. In the midst of a PhD, I cannot emphasize enough how important revisiting this sentiment was in helping me cope and manage stress in the midst of imposter syndrome, fears of public speaking, deadlines and other academic pressures. My mom has lived with a chronic autoimmune disease since before I was born and is my greatest inspiration. You are what motivates me to do this every

day. Thank you for all of the sacrifices you've made so that I could realize this achievement.

And finally, my deepest thank you to Christian, my partner in life. Thank you for keeping me fed during long days and nights working on my paper. Thank you for supporting me in every way, for lifting me up during the difficult times and helping me celebrate every success. Thank you for always making me laugh and for being a better friend, confidant and companion than I could have ever imagined I would have the opportunity to spend my life with. I love you so much.

Contributions to this work

The work presented in this dissertation was performed under the supervision and guidance of Dr. Alexander Marson, MD, PhD. Guidance and insight were provided by thesis committee members Dr. Mark Anderson, MD, PhD and Dr. K. Mark Ansel, PhD. Additional suggestions were provided by Dr. Jeffrey Bluestone, PhD.

Chapters 2 and 3 of this work are adopted from a collaborative effort with Deyu Fang's lab (Northwestern) as it appears in the following publication:

Cortez JT, Montauti E, Shifrut E, Gatchalian J, Zhang Y, Shaked O, Xu Y, Roth TL, Simeonov DR, Zhang Y, Chen S, Li Z, Woo JM, Ho J, Vogel IA, Prator GY, Zhang B, Lee Y, Sun Z, Ifergan I, Van Gool F, Hargreaves DC, Bluestone JA, Marson A, Fang D. CRISPR screen in regulatory T cells reveals modulators of Foxp3. *Nature*.

doi: <http://dx.doi.org/10.1038/s41586-020-2246-4>

Conceptualization: J.T.C., E.M., E.S., Yu.Z., Z.S., F.V.G., J.A.B., A.M., D.F. Methodology: J.T.C., E.S., T.L.R. Investigation: J.T.C., E.M., E.S., J.G., Yu.Z., O.S., Y.X., T.L.R., D.R.S., Ya.Z., S.C., Z.L., J.M.W., J.H., I.A.V., G.Y.P., Y.L., I.I. Resources: D.C.H., J.A.B., A.M., D.F. Formal analysis: J.T.C., E.S., J.G. Software: E.S. Data Curation: J.T.C., E.S., J.G. Supervision: B.Z., Y.L., F.V.G., D.C.H., J.A.B., A.M., D.F. Funding acquisition: J.T.C., E.M., D.C.H., A.M., D.F. Writing – original draft preparation: J.T.C., E.M., J.G., Yu.Z., A.M., D.F. Writing – review and editing: J.T.C., E.M., J.G., Z.S., F.V.G., D.C.H., J.A.B., A.M., D.F.

CRISPR screen in regulatory T cells reveals modulators of Foxp3

Jessica T. Cortez

Abstract

Regulatory T cells (Tregs) are required to control immune responses and maintain homeostasis, but are a significant barrier to anti-tumor immunity¹. Conversely, Treg instability, characterized by loss of the master transcription factor Foxp3 and acquisition of pro-inflammatory properties², can promote autoimmunity and/or facilitate more effective tumor immunity^{3,4}. A comprehensive understanding of the pathways that regulate Foxp3 could lead to more effective Treg therapies for autoimmune disease and cancer. Despite improved functional genetic tools that now allow for systematic interrogation, dissection of the gene regulatory programs that modulate Foxp3 expression has not yet been reported. In this study, we developed a CRISPR-based pooled screening platform for phenotypes in primary mouse Tregs and applied this technology to perform a targeted loss-of-function screen of ~490 nuclear factors to identify gene regulatory programs that promote or disrupt Foxp3 expression. We discovered several novel modulators including ubiquitin-specific peptidase 22 (Usp22) and ring finger protein 20 (Rnf20). Usp22, a member of the deubiquitination module of the SAGA chromatin modifying complex, was discovered to be a positive regulator that stabilized Foxp3 expression; whereas the screen suggested Rnf20, an E3 ubiquitin ligase, can serve as a negative regulator of Foxp3. Treg-specific ablation of Usp22 in mice reduced Foxp3 protein and created defects in their suppressive function that led to spontaneous autoimmunity but protected against tumor growth in multiple cancer models. Foxp3 destabilization in Usp22-deficient Tregs could be rescued by ablation of Rnf20, revealing

a reciprocal ubiquitin switch in Tregs. These results reveal novel modulators of Foxp3 and demonstrate a screening method that can be broadly applied to discover new targets for Treg immunotherapies for cancer and autoimmune disease.

Table of Contents

CHAPTER 1: INTRODUCTION 1

 Regulatory T cell function and stability.....2

 CRISPR tools to systematically interrogate immune function3

**CHAPTER 2: CRISPR SCREEN IN REGULATORY T CELLS REVEALS
MODULATORS OF FOXP3.....4**

 Discovery and validation of Foxp3 regulators in primary Tregs using a pooled
 CRISPR screen.....5

 Usp22 is required for Foxp3 maintenance and Treg suppressive function.....7

 Usp22 regulates Foxp3 through transcriptional mechanisms mediated via
 deubiquitination of histone 2B8

 Usp22 and Rnf20 act as reciprocal regulators of Foxp3..... 10

 Treg-specific ablation of Usp22 results in autoimmunity and enhances anti-
 tumor immunity..... 11

 Summary..... 13

 Acknowledgements 14

 Figures 16

 Tables.....37

CHAPTER 3: METHODS 45

 Mice for screen and RNP validation.....46

Isolation and culture of primary mouse Tregs for screen and validation	46
Pooled sgRNA library design and construction	47
Retrovirus production	47
Retroviral transduction	48
Foxp3 intracellular stain and post-screen cell collection	49
Isolation of genomic DNA from fixed cells	49
Preparation of genomic DNA for next generation sequencing	50
Pooled CRISPR screen pipeline	51
Analysis of pooled CRISPR screen	51
Arrayed Cas9 ribonucleotide protein (RNP) preparation and electroporation ...	52
PCR amplification of target regions and TIDE analysis	53
Isolation, culture and FOXP3 intracellular staining of human Treg cells	54
Generation of Usp22 knockout mice	55
Cell lines, plasmids, antibodies, and reagents	56
Cell isolation and flow cytometry for analysis of Usp22 mice	57
Tumor models	57
<i>In vitro</i> Treg suppression assay	58
Rescue experiment with Foxp3 overexpression	58
Induced Treg (iTreg) differentiation	59

Th1, Th2 and Th17 <i>in vitro</i> differentiations	60
Quantitative PCR (qPCR)	60
Histology.....	60
Co-Immunoprecipitation and Western blot	60
Ubiquitination assay.....	61
ChIP-qPCR sample preparation.....	62
ChIP-seq sample preparation	63
ChIP-seq analysis	64
RNA sequencing	66
Adoptive transfer model of colitis.....	67
Induced experimental autoimmune encephalomyelitis (EAE).....	67
Data availability.....	68
CHAPTER 4: CONCLUDING REMARKS	69
Future directions.....	70
The future of Treg cell therapies	70
REFERENCES.....	71

List of Figures

Figure 2.1. Discovery and validation Foxp3 regulators in primary Tregs using a pooled CRISPR screen.	16
Figure 2.2. Usp22 is required for Foxp3 maintenance and Treg suppressive function.	18
Figure 2.3. Treg-specific ablation of Usp22 results in autoimmunity and enhances anti-tumor immunity.....	20
Figure 2.4. Design and quality control of targeted pooled CRISPR screen in primary mouse Tregs.....	22
Figure 2.5. Validation of Foxp3 modulators in primary mouse and human Tregs with Cas9 RNP electroporation.....	24
Figure 2.6. Design and validation of Treg-specific Usp22 knockout mice.	26
Figure 2.7. Usp22 acts as deubiquitinase to control post-translational Foxp3 expression.	28
Figure 2.8. Usp22 regulates Foxp3 through transcriptional mechanisms.....	29
Figure 2.9. Autoimmune inflammation in Treg-specific Usp22 knockout mice.....	32
Figure 2.10. T cell-specific ablation of Usp22 resulted in decreased Foxp3 and increased T cell activation.	33
Figure 2.11. Tumor growth is inhibited in Treg-specific Usp22 knockout mice in multiple cancer models.	35

List of Tables

Table 2.1. Top 30 gene level hits from screen data.....	37
Table 2.2. List of primers	38
Table 2.3. List of crRNA	40
Table 2.4. List of Antibodies.....	42

CHAPTER 1: INTRODUCTION

Regulatory T cell function and stability

Regulatory T cells (Tregs) are a specialized subset of CD4⁺ T cells that function to suppress immune responses and maintain self-tolerance¹. Stable expression of the transcription factor Forkhead box P3 (Foxp3) in Tregs ensures robust suppressive function in inflammatory environments. Tregs have previously been thought to be irreversibly committed to suppressive functions⁵, however, lineage tracing studies challenged this by revealing that Tregs exhibit plasticity. Tregs that lose Foxp3 expression, termed exTregs, can acquire proinflammatory cytokine production capabilities similar to effector T cells and exacerbate autoimmunity². These findings raise questions of lineage compartmentalization and cellular plasticity among CD4⁺ T cell subsets. While exTregs that produce higher amounts of pro-inflammatory cytokines can lead to rapid and fatal onset of autoimmunity, the deterioration of Treg function provides an advantage in developing more effective anti-tumor immune responses⁶. A better understanding of the fundamental regulators of Foxp3 instability is key to being able to manipulate Treg function as a therapeutic intervention.

The Treg suppressive phenotype is largely driven by gene expression patterns dictated by Foxp3. Control of Foxp3 stability, and thus Treg function, is thought to occur at both the transcriptional and post-translational level. Epigenetic modifications at the *Foxp3* locus and at Treg-associated loci can affect Foxp3 transcription and facilitate the generation of ex-Foxp3 Tregs⁷. Foxp3 protein can also be dynamically controlled post-translationally by deubiquitinases (DUBs) or ubiquitin ligases in response to proinflammatory signals⁸. Despite years of work to understand and identify regulators of

Foxp3 expression, the field still lacks systematic strategies to comprehensively interrogate genes that control Treg identity and function. There is a critical need to identify factors that manipulate Foxp3 expression in order to provide rapid and temporal control of Treg function.

CRISPR tools to systematically interrogate immune function

Recent advances in CRISPR-Cas9 technology have overcome the major challenge of effective genetic perturbation to perform high-throughput genetic studies. Although the development of commercially available lentiviral single guide RNA (sgRNA) libraries and Cas9 knock-in mice⁹ have enabled screens in other primary cell types^{10,11}, large-scale screens in murine Tregs have yet to be achieved.

**CHAPTER 2: CRISPR SCREEN IN REGULATORY T CELLS REVEALS
MODULATORS OF FOXP3**

Discovery and validation of Foxp3 regulators in primary Tregs using a pooled CRISPR screen

While unstable Foxp3 expression in Tregs can result in autoimmunity, similar changes that reduce Treg suppressive function can contribute to more effective anti-tumor immune responses⁴. Understanding the fundamental regulators of Foxp3 is critical, especially as we navigate towards new potential applications for Treg therapies to treat autoimmunity and cancer¹².

To discover novel regulators of Foxp3 stability, we developed a pooled CRISPR screening platform in primary mouse Tregs (**Fig. 1a**). We first designed a targeted library of ~490 nuclear factors based on optimized single guide RNA (sgRNA) sequences from the Brie library¹³ (**Fig. 4a**) and used a retroviral vector to introduce this library into *ex vivo* Tregs isolated from *Foxp3*^{GFP-Cre}*Rosa26*^{LSL-RFP}*Cas9* mice (**Fig. 4b-4e**). We then stained for endogenous Foxp3 protein and sorted the highest Foxp3-expressing cells (Foxp3^{high}) and the lowest (Foxp3^{low}). MAGeCK software¹⁴ systematically identified sgRNAs that were enriched or depleted in Foxp3^{low} cells relative to Foxp3^{high} cells (**Table 1**). We were able to maintain high sgRNA coverage of our library (~1000x) and non-targeting control (NTC) sgRNAs showed no effect (**Figs. 4f, 4g**) which provided confidence that our hits identified biological pathways controlling Foxp3 levels.

Our screen revealed many novel Foxp3 regulators, with a bias towards identifying positive regulators over negative regulators (**Figs. 1b, 1c**). sgRNAs enriched in the Foxp3^{low}

population reflect positive regulators (blue) that promote Foxp3 expression while sgRNAs depleted in the Foxp3^{low} population reflect negative regulators (red) that inhibit Foxp3 expression. As expected, sgRNAs targeting *Foxp3* were enriched in the Foxp3^{low} population. We also identified many established regulators known to be important for maintenance of Foxp3 expression including *Cbfb*, *Runx1* and *Stat5b*^{7,15–21} as positive regulators and *Sp3* and *Satb1* as negative regulators^{7,21} providing further confidence in our hits. Importantly, several novel factors and complexes that modulate Foxp3 were identified including positive regulators *Usp22*, *Atxn7l3* and negative regulator *Rnf20*. The deubiquitinase (DUB) *Usp22* and cofactor *Atxn7l3*, are both members of deubiquitination module of the SAGA chromatin modifying complex²² (**Fig. 4h**).

To validate the effects of our screen hits on Foxp3 levels, we assessed five of the top-ranking positive regulators by individual CRISPR knockout with Cas9 ribonucleoproteins²³ (RNPs) (**Fig. 8a**). The effects on Foxp3 levels were consistent across multiple guide RNAs (gRNAs) targeting the key candidate regulators (**Fig. 1d, Figs. 5b-d and Table 2**). These results strongly confirmed the candidate genes identified from our screen as positive regulators of Foxp3. As our screen indicated that *Usp22* is a positive regulator of Foxp3, we next wanted to assess the potential therapeutic relevance of *USP22* by knocking it out with RNPs in human Tregs. We saw a significant decrease in FOXP3 mean fluorescence intensity (MFI) (**Figs. 1e, 1f**) and frequencies of FOXP3⁺ and FOXP3^{hi}CD25^{hi} cells in *USP22*-targeted human Tregs (**Figs. 5e-g**) across experiments performed in ten different blood donors. The effects of *USP22* targeting in human Tregs on FOXP3 levels were also observed with multiple distinct gRNAs (**Figs.**

5h-j). Together these findings confirm critical regulation of Foxp3 by members of the SAGA complex, especially Usp22.

Usp22 is required for Foxp3 maintenance and Treg suppressive function.

To understand the *in vivo* significance of Usp22 in Tregs, we generated mice with Treg-specific ablation of Usp22 by creating *Usp22^{fl/fl}* mice (**Figs. 6a, 6b**) and crossing them with *Foxp3^{YFP-Cre}* mice²⁴. Western blot analysis confirmed specific deletion of Usp22 in Treg cells, but not in CD4⁺ conventional T (Tconv) cells (**Fig. 6c**). *Usp22^{fl/fl}Foxp3^{YFP-Cre}* knockout (KO) mice had a marked decrease in Foxp3 MFI in Tregs isolated from spleens, thymus and peripheral lymph nodes (pLN) (**Figs. 2a-c**) compared to *Usp22^{+/+}Foxp3^{YFP-Cre}* wild-type (WT) mice, as well as decreased Treg frequencies (**Fig. 6d**). Western blot analysis confirmed a significant reduction in Foxp3 protein in Usp22-null Tregs (**Fig. 6e**). A decrease in Foxp3⁺ cells was also seen in induced Tregs (iTregs), although less pronounced with increasing levels of TGF- β (**Figs. 6f, 6g**). Given the diminished Foxp3 levels in Usp22 KO Tregs, we reasoned that these cells may exhibit defects in suppressive function. Indeed, Usp22 KO Tregs were less able to suppress T effector cells than WT Tregs from *Usp22^{+/+}Foxp3^{YFP-Cre}* mice (**Fig. 2d, Fig. 6h**), and this defect could be rescued by heterologous expression of Foxp3 (**Figs. 6i, 6j**). These data substantiate our screen data and suggest Usp22 promotes Foxp3 levels and is critical for Treg function.

Usp22 regulates Foxp3 through transcriptional mechanisms mediated via deubiquitination of histone 2B

Control of Foxp3 stability, and thus Treg function, can occur at the transcriptional and/or post-transcriptional level²⁵. Chromatin modifications at the *Foxp3* locus and other key loci can affect Foxp3 transcription^{26–31}. As Usp22 is a component of the chromatin modifying SAGA complex, we hypothesized that Usp22 controls Foxp3 expression through transcriptional regulation. IRES-YFP knock-in to the *Foxp3* locus of *Usp22^{fl/fl}Foxp3^{YFP-Cre}* mice allowed us to use YFP as a reporter to assess the effect of Usp22 on *Foxp3* transcript levels. Similar to endogenous Foxp3 protein, YFP MFI was significantly decreased in Usp22-null Tregs isolated from the thymus, pLN and spleen in *Usp22^{fl/fl}Foxp3^{YFP-Cre}* mice compared to *Usp22^{+/+}Foxp3^{YFP-Cre}* mice, despite normal Treg frequencies (**Figs. 2e, 8a-c**). Furthermore, by qPCR, *Foxp3* transcripts were significantly reduced in splenic Tregs from *Usp22^{fl/fl}Foxp3^{YFP-Cre}* compared to *Usp22^{+/+}Foxp3^{YFP-Cre}* mice (**Fig. 2f**). RNA sequencing confirmed that *Foxp3* transcripts are significantly reduced in Tregs from *Usp22^{fl/fl}Foxp3^{YFP-Cre}* mice relative to WT (**Fig. 2g**). *Foxp3* transcript levels also trended down with acute targeting by Usp22 RNPs in mouse and human Tregs, although results were less consistent perhaps due to variability in knockout efficiency and/or other experimental factors (**Figs. 8d-f**). Foxp3 protein can also be dynamically controlled post-translationally by DUBs or ubiquitin ligases in response to proinflammatory signals^{8,32–35}. We investigated whether Foxp3 protein can be directly targeted by Usp22. Usp22 loss contributed to increased Foxp3 ubiquitination and

degradation (**Fig. 7**). These results are consistent with *Usp22* tuning *Foxp3* expression at transcriptional and post-transcriptional levels.

Usp22 is required for SAGA-mediated deubiquitination of histones, which regulates transcriptional activity³⁶. We therefore tested if histone ubiquitination was altered in *Usp22* KO Tregs. Western blot analysis confirmed that *Usp22^{fl/fl}Foxp3^{YFP-Cre}* mice had increased levels of ubiquitinated histone 2A and 2B (H2AK119Ub and H2BK120Ub, respectively) in iTregs compared to *Usp22^{+/+}Foxp3^{YFP-Cre}* mice (**Fig. 8g**). Chromatin immunoprecipitation followed by qPCR (ChIP-qPCR) showed increased H2BK120Ub in the conserved non-coding sequence 1 (CNS1) region of the *Foxp3* locus in *Usp22^{fl/fl}Foxp3^{YFP-Cre}* Tregs, whereas effects on H2AK119Ub levels at the locus were not significant (**Figs. 8h-j**). Further interrogation with ChIP followed by genome-wide sequencing (ChIP-seq) revealed significant increases in H2BK120Ub levels across the *Foxp3* locus in *Usp22^{fl/fl}Foxp3^{YFP-Cre}* Tregs compared with control Tregs. A significant accumulation of H2BK120Ub at the locus also was observed in Tregs electroporated with *Usp22* Cas9 RNPs compared to those treated with NTC Cas9 RNPs (**Fig. 2h**). These findings demonstrated that *Usp22* is essential for chromatin regulation at the *Foxp3* locus.

We next analyzed effects of *Usp22* loss on chromatin states across the Treg genome. First, we found evidence that *Usp22* can co-occupy many *Foxp3*-bound regions in Tregs (**Fig. 8k**). *Foxp3*-bound regions tended to gain H2BK120Ub in *Usp22*-deficient cells compared to control cells and increases in H2BK120Ub were more pronounced than effects on H2AK119Ub, suggesting that H2BK120Ub is likely the more relevant chromatin

target of Usp22 in Tregs (**Fig. 2h, 8k**). Looking more broadly across the genome, we found that sites that significantly gained H2BK120Ub in both Usp22KO and Usp22-RNP targeted Tregs were enriched for activating histone modifications (H3K4me3, H3K4me and H3K27ac) suggesting that changes occurred at gene regulatory elements, including at Treg-specific super enhancers (**Figs. 8l, 8m**). These data revealed a critical role for Usp22 in control of H2KB120Ub across the Treg chromatin landscape.

Usp22 and Rnf20 act as reciprocal regulators of Foxp3

Our screen nominated E3-ubiquitin ligase Rnf20 as a candidate negative regulator of Foxp3. We hypothesized that the DUB Usp22 and E3-ubiquitin ligase Rnf20 might have an epistatic relationship given their reciprocal effects on histone ubiquitination. To test this, we used RNPs to knockout Rnf20 in Usp22 KO or WT Tregs. Although Cas9 RNP-mediated loss of Rnf20 alone did not significantly increase Foxp3 levels in WT Tregs (**Figs. 2h, 5d**), Rnf20 RNP knockout was able to rescue the impairment in *Foxp3* transcript levels (assessed by YFP levels) in Usp22-deficient Tregs (**Fig. 8n**). Double RNP knockout of both USP22 and RNF20 in mouse and human Tregs also rescued FOXP3 protein levels relative to USP22 RNP treatment alone, although effects on transcript levels were less consistent (**Figs. 2i, 5h, 5j, 8e, 8f**). Consistent with a model where the ubiquitin ligase Rnf20 and DUB Usp22 have reciprocal functional roles, we found that Rnf20 co-occupies Foxp3-bound regions (**Fig. 8k**). Although Rnf20 ablation did not affect already low levels of H2BK120Ub at the Foxp3 locus, targeting Rnf20 tended to reduce H2BK120Ub levels at these Foxp3-bound regions genome-wide

whereas Usp22 deficiency increased them (**Fig. 2h, 8k**). Western blot analysis confirmed that targeting Rnf20 in Usp22-deficient cells restored H2BK120Ub levels back to those of control Tregs (**Fig. 2j**). Taken together, these results revealed reciprocal regulation of Foxp3 and key chromatin regions in Tregs by Usp22 and Rnf20.

Treg-specific ablation of Usp22 results in autoimmunity and enhances anti-tumor immunity

To determine the *in vivo* functional relevance of Usp22 deficiency in Tregs, we characterized the spontaneous autoimmune symptoms of *Usp22^{fl/fl}Foxp3^{YFP-Cre}* mice. While *Usp22^{fl/fl}Foxp3^{YFP-Cre}* mice were born at normal size, their body weights were lower than those of age and sex matched *Usp22^{+/+}Foxp3^{YFP-Cre}* mice after 5 weeks of age (**Figs. 3a, 9a**). We next assessed whether this body weight reduction might be due to chronic inflammation as is observed with impaired Treg function¹. Indeed, flow cytometry analysis detected greater frequencies of CD4⁺ and CD8⁺ effector memory T cells (CD44^{hi}CD62L^{lo}) and corresponding lower percentages of naïve T cells (CD44^{lo}CD62L^{hi}) in 7-month-old KO mice compared to WT (**Figs. 9b, 9c**). Additionally, histological analysis of aged mice detected lymphocyte infiltration in multiple organs, including kidney, lung, colon and liver (**Fig. 3b**). Importantly, ablation of Usp22 in all T cells in *Usp22^{fl/fl}Lck^{Cre}* mice largely phenocopied the reduced levels of Foxp3 in Tregs and lymphoproliferation observed in the *Usp22^{fl/fl}Foxp3^{YFP-Cre}* mice (**Fig. 10**). These findings underscored a relatively selective role of Usp22 in Foxp3 regulation and Treg suppressive function, rather than global requirement for Usp22 in T cell function.

We further validated the *in vivo* requirements for Usp22 in Treg suppressive function using multiple models of autoimmune disease. We assessed Treg suppressive activity *in vivo* using an adoptive transfer model of colitis and a MOG-induced experimental autoimmune encephalomyelitis (EAE) model. In the colitis model, mice that received defective Usp22 KO Tregs were not protected against colitis, in contrast to those that received WT Tregs (**Figs. 3c, 3d**). Similarly, in the EAE model, *Usp22^{fl/fl}Foxp3^{YFP-Cre}* mice showed worse clinical scores compared to WT mice suggesting an inability of the Usp22-deficient Tregs to limit autoimmunity (**Fig. 3e**).

Since these data suggest that Usp22 deficiency reduces Foxp3 stability and impairs Treg suppressive function, we next tested whether *Usp22^{fl/fl}Foxp3^{YFP-Cre}* mice would exhibit increased anti-tumor immunity using syngeneic tumor models. As expected, growth of EG7 lymphoma tumors was significantly inhibited by Treg-specific Usp22 gene deletion (**Fig. 3f**). We next examined the immune responses in these tumor-bearing mice and found greater proportions of effector-memory CD4⁺ and CD8⁺ T cells in the spleens of *Usp22^{fl/fl}Foxp3^{YFP-Cre}* mice compared to WT (**Figs. 3g, 3h**). We also found increased frequencies of interferon- γ (IFN γ) and granzyme B producing CD8⁺ T cells, as well as increased mRNA levels of *Irfng*, *Gzmb* and *Cd8a* from tumor tissue (**Fig. 11d**), suggesting an increased cytotoxic lymphocyte response due to impaired Treg suppressive function. Splenic Tregs from these mice showed reduced MFIs of Foxp3 target genes important for Treg function including CD25 (**Figs. 11a-c**). Further analysis of tumor-infiltrating lymphocytes indicated a significant increase in CD8⁺ T cell frequencies and decreased

percentages of intratumoral Foxp3⁺ Tregs in EG7 tumor-bearing *Usp22^{fl/fl}Foxp3^{YFP-Cre}* mice (**Fig. 3i-j**). Consistent with the lymphoid organs, we found that the Foxp3 MFI was significantly decreased in the intratumoral Treg cells from EG7 tumor-bearing KO mice (**Fig. 3k**). Taken together, these data indicate Usp22 KO impairs Treg suppressive function and reduces Treg abundance in EG7 tumors, consequently enhancing the anti-tumor immune response. We also showed that *Usp22^{fl/fl}Foxp3^{YFP-Cre}* mice exhibit increased anti-tumor immunity in additional tumor models (**Figs. 11e-m**). These results highlight Usp22 in Tregs as a new potential target for anti-tumor immunotherapies.

Summary

Here, we developed the first CRISPR-based pooled screening platform for primary mouse Tregs and applied this technology for systematic identification of gene modifications that control Foxp3 levels. We discovered several novel regulators of Foxp3 including Usp22 and Rnf20. We developed a Treg-specific Usp22 KO mouse and showed that Usp22 is critical to stabilize Foxp3 and maintain suppressive functions *in vivo*. We demonstrate that Usp22 is a regulator of *Foxp3* transcript levels, likely through deubiquitination of H2B at *Foxp3* and other key loci, and that Usp22 can also regulate Foxp3 post-translationally. Mice with Usp22-null Tregs showed impaired ability to resolve autoimmune inflammation and an enhanced anti-tumor immune response. Usp22 could be a particularly attractive cancer immunotherapy target because in addition to its role in Tregs that can limit anti-tumor immune responses, over-expression of Usp22 in cancer cells is associated with poor prognosis in a variety of tumor types³⁷ and Usp22 knockdown in cancer cells can

induce their apoptosis³⁸. This study provides a resource of novel Foxp3 regulators that can be perturbed to fine tune Treg function and specifically defines the function of Usp22 and Rnf20 as important modulators of Foxp3 and potential targets for Treg immunotherapies.

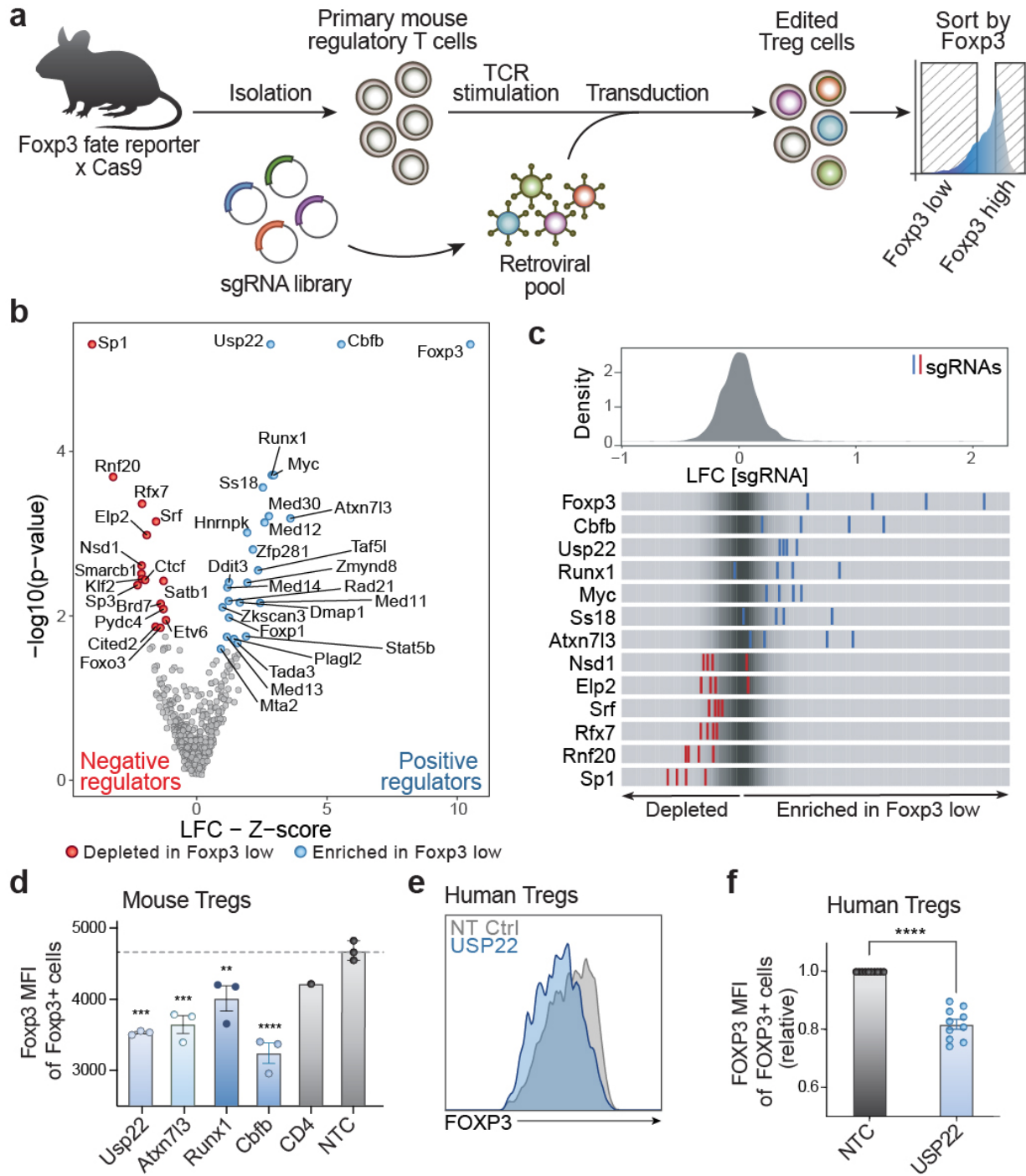
Acknowledgements

We thank all members of the Marson lab as well as Mark S. Anderson, K. Mark Ansel, Chun J. Ye, Kathrin Schumann and Luke Gilbert for helpful suggestions and technical advice. We thank Jacob Freimer, Siddharth Raju and Eric Guo for helpful advice and assistance with the RNA-seq analysis pipeline. We thank Vinh Nguyen, Victoria Tobin, Ryan Apathy, Michelle Nguyen, the UCSF Flow Cytometry Core, and Nasun Hah and Grace Chou in the Salk NGS Core Facility for technical assistance. We thank Sarah Pyle for assistance with graphics. We thank David Nguyen for critical reading of the manuscript. J.T.C. is supported by the National Science Foundation Graduate Research Fellowship Program grant 1650113. J.G. was supported by the Salk Institute T32 Cancer Training Grant T32CA009370 and the NIGMS NRSA F32 GM128377-01. D.C.H. is supported by the National Institutes of Health (NIH) (GM128943-01, CA184043-03), the V Foundation for Cancer Research V2016-006, the Pew-Stewart Foundation for Cancer Research, and the Leona M. and Harry B. Helmsley Charitable Trust. The Marson lab has received gifts from J. Aronov, G. Hoskin, K. Jordan, B. Bakar, the Caufield family and funds from the Innovative Genomics Institute (IGI) and the Parker Institute for Cancer Immunotherapy (PICI). A.M. holds a Career Award for

Medical Scientists from the Burroughs Wellcome Fund, is an investigator at the Chan Zuckerberg Biohub and is a recipient of a The Cancer Research Institute (CRI) Lloyd J. Old STAR grant. This work used the Vincent J. Coates Genomics Sequencing Laboratory at UC Berkeley, supported by NIH S10 OD018174 Instrumentation Grant, the UCSF Flow Cytometry Core, supported by the Diabetes Research Center grants NIH P30 DK063720 and NIH S10 1S10OD021822-01, and the Salk NGS Core Facility, supported by the NIH-NCI CCSG: P30 014195, the Chapman Foundation, and the Helmsley Charitable Trust. D.F. is supported by NIH R01 grants (AI079056, AI108634 and CA232347). E.M. is supported by NIH F31 CA220801-03.

Figures

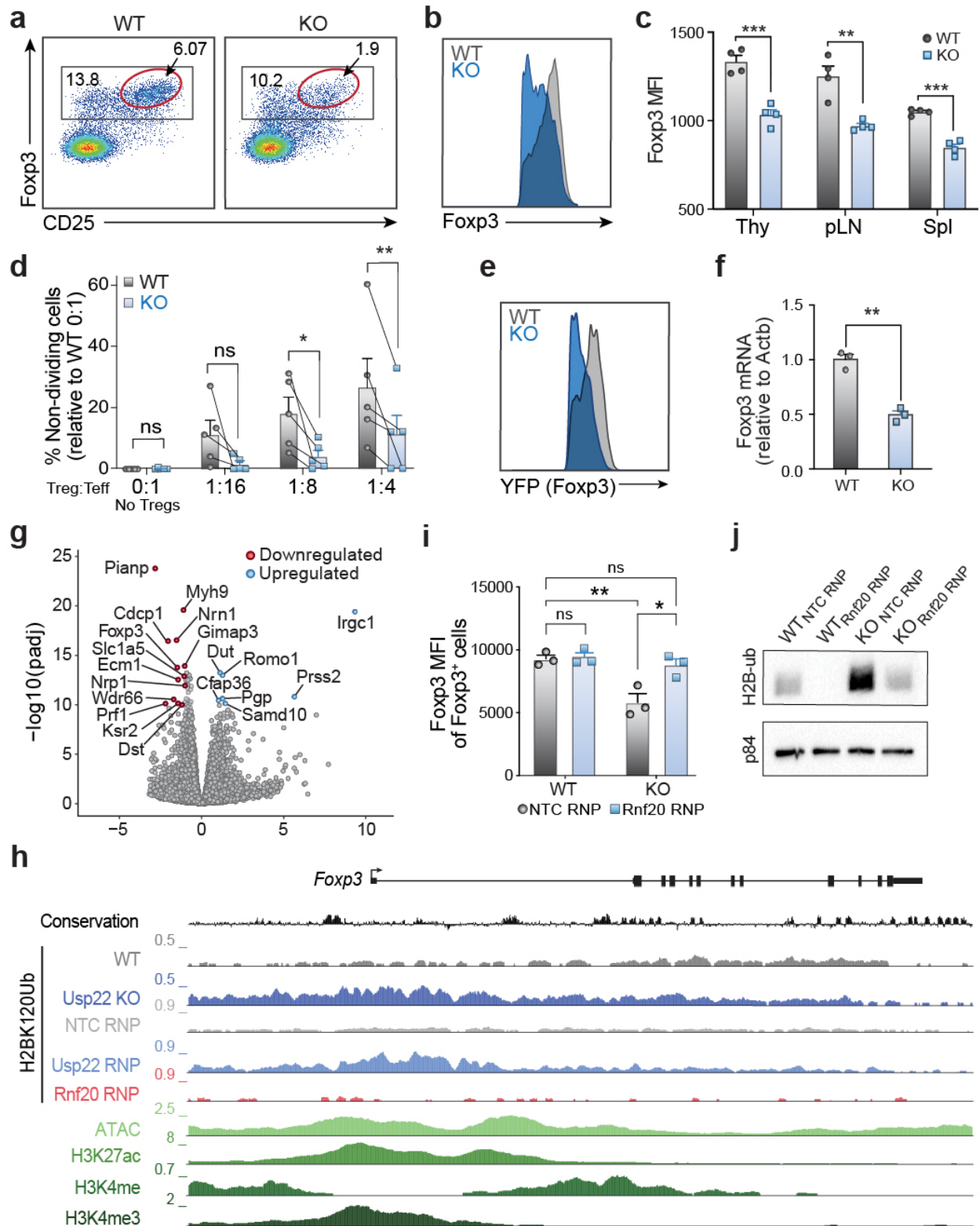
Figure 2.1. Discovery and validation FoXP3 regulators in primary Tregs using a pooled CRISPR screen.



- a) Diagram of pooled CRISPR screening platform in primary mouse Treg cells.
- b) Volcano plot for hits from the screen. X-axis shows Z-score for gene-level log₂ fold-change (LFC); median of LFC for all single guide RNAs (sgRNAs) per gene, scaled. Y-axis shows the p-value as calculated by MAGeCK⁷. Red are negative regulators (depleted in Foxp3 low cells), while blue dots show all positive regulators (enriched in Foxp3 low cells) defined by FDR < 0.5 and Z-score > 0.5.
- c) Top panel: distribution of sgRNA-level LFC values of Foxp3 low over Foxp3 high cells for 2,000 guides. Bottom panel: LFC for all four individual sgRNAs targeting genes enriched in Foxp3 low cells (blue lines) and depleted genes (red lines), overlaid on grey gradient depicting the overall distribution.
- d) Mean fluorescence intensity (MFI) of Foxp3 in Foxp3⁺ cells from data in Fig. 5b. Each data point represents effects of an independent gRNA for each target gene. Statistics are based on comparison to non-targeting control (NTC).
- e) Representative histogram showing FOXP3 MFI (pre-gated on live cells) from human Tregs treated with non-targeting control (NTC) or USP22 Cas9 RNPs.
- f) Statistical analysis of FOXP3 MFI in human Tregs from 10 biological replicates. Tregs from each donor here were targeted with the same high efficiency gRNA (USP22-2).

All data are presented as mean \pm SEM. ns indicates no significant difference, *P < 0.05, **P < 0.01, ***P < 0.001, ****P < 0.0001.

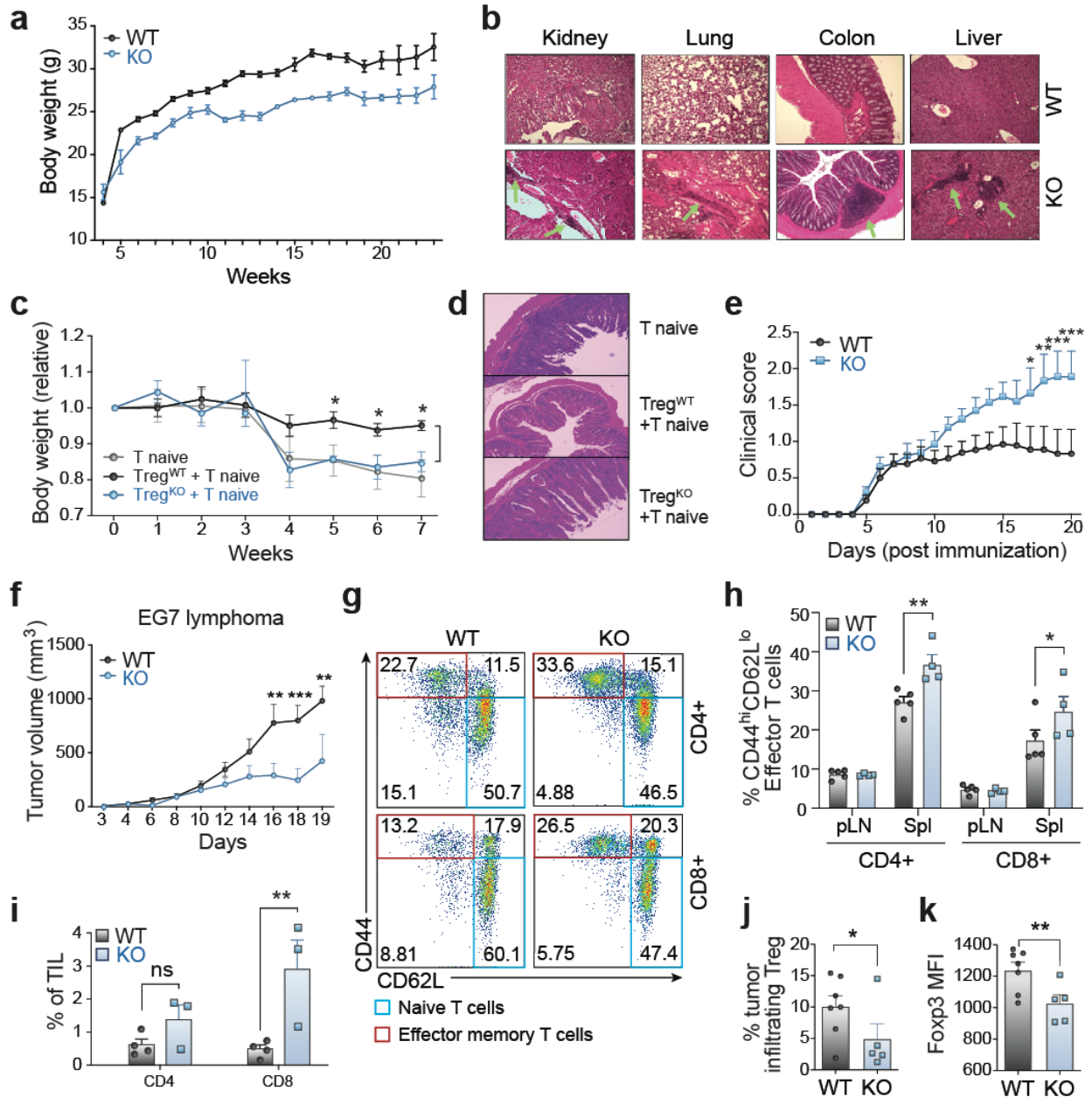
Figure 2.2. Usp22 is required for Foxp3 maintenance and Treg suppressive function.



- a) Representative flow cytometry analysis of the Treg population (gated on CD4⁺ cells) from the spleen of *Usp22*^{+/+}*Foxp3*^{YFP-Cre} WT or *Usp22*^{fl/fl}*Foxp3*^{YFP-Cre} KO mice. A subset of Tregs with the highest expression of Foxp3 and CD25 is highlighted with a red gate.
- b) Histogram of Foxp3 expression in Foxp3⁺ Tregs from spleens of *Usp22*^{+/+}*Foxp3*^{YFP-Cre} WT or *Usp22*^{fl/fl}*Foxp3*^{YFP-Cre} KO mice from panel a.
- c) Statistical analysis of Foxp3 MFI from CD4⁺Foxp3⁺ Tregs in thymus (Thy), peripheral lymph nodes (pLN) and spleen (Spl) of *Usp22*^{+/+}*Foxp3*^{YFP-Cre} WT or *Usp22*^{fl/fl}*Foxp3*^{YFP-Cre} KO mice.
- d) Summary data of *in vitro* suppression experiments, corresponding to Fig. 6h. Lines connect paired samples. Data are presented as the frequency of non-dividing cells relative to WT 0:1 No Treg control, with any negative values after normalization replaced with 0.
- e) Histogram of YFP expression in Tregs from the spleen and lymph nodes of *Usp22*^{+/+}*Foxp3*^{YFP-Cre} WT or *Usp22*^{fl/fl}*Foxp3*^{YFP-Cre} KO mice from Fig. 8a.
- f) qPCR analysis of Foxp3 mRNA levels in sorted YFP⁺ cells of spleen from *Usp22*^{+/+}*Foxp3*^{YFP-Cre} WT or *Usp22*^{fl/fl}*Foxp3*^{YFP-Cre} KO mice.
- g) Volcano plot for RNA sequencing of YFP⁺ Tregs sorted from *Usp22*^{+/+}*Foxp3*^{YFP-Cre} WT or *Usp22*^{fl/fl}*Foxp3*^{YFP-Cre} KO mice. X-axis shows log2FoldChange (LFC). Y-axis shows the $-\log_{10}$ of the adjusted p-value (padj) as calculated by DESeq2. Genes downregulated in the KO are shown in red and genes upregulated are shown in blue defined by padj < 1e-10 and LFC > 1.
- h) Genome tracks of ChIP-seq for H2BK120Ub at the *Foxp3* locus in wild-type (WT), *Usp22* KO, non-targeting control (NTC-RNP) treated, *Usp22*-RNP treated and Rnf20-RNP treated Tregs. Evolutionary conservation, ATAC-seq, and ChIP-Seq for H3K27ac, H3K4me3, and H3K4me in WT Tregs are also shown.
- i) Analysis of reciprocal regulation of Foxp3 by deubiquitinase *Usp22* and E3 ubiquitin ligase Rnf20. Foxp3 MFI of Tregs sorted from *Usp22*^{+/+}*Foxp3*^{YFP-Cre} WT or *Usp22*^{fl/fl}*Foxp3*^{YFP-Cre} KO mice and then electroporated with either NT control (NTC-RNP) or Rnf20 RNP.
- j) Western blot analysis of H2BK120Ub (H2B-ub) levels in Tregs sorted from *Usp22*^{+/+}*Foxp3*^{YFP-Cre} WT or *Usp22*^{fl/fl}*Foxp3*^{YFP-Cre} KO mice and then electroporated with either NT control (NTC-RNP) or Rnf20 RNP; corresponding to panel i. p84 was used as a loading control.

All data are presented as mean \pm SEM. ns indicates no significant difference, *P < 0.05, **P < 0.01, ***P < 0.001, ****P < 0.0001.

Figure 2.3. Treg-specific ablation of *Usp22* results in autoimmunity and enhances anti-tumor immunity.



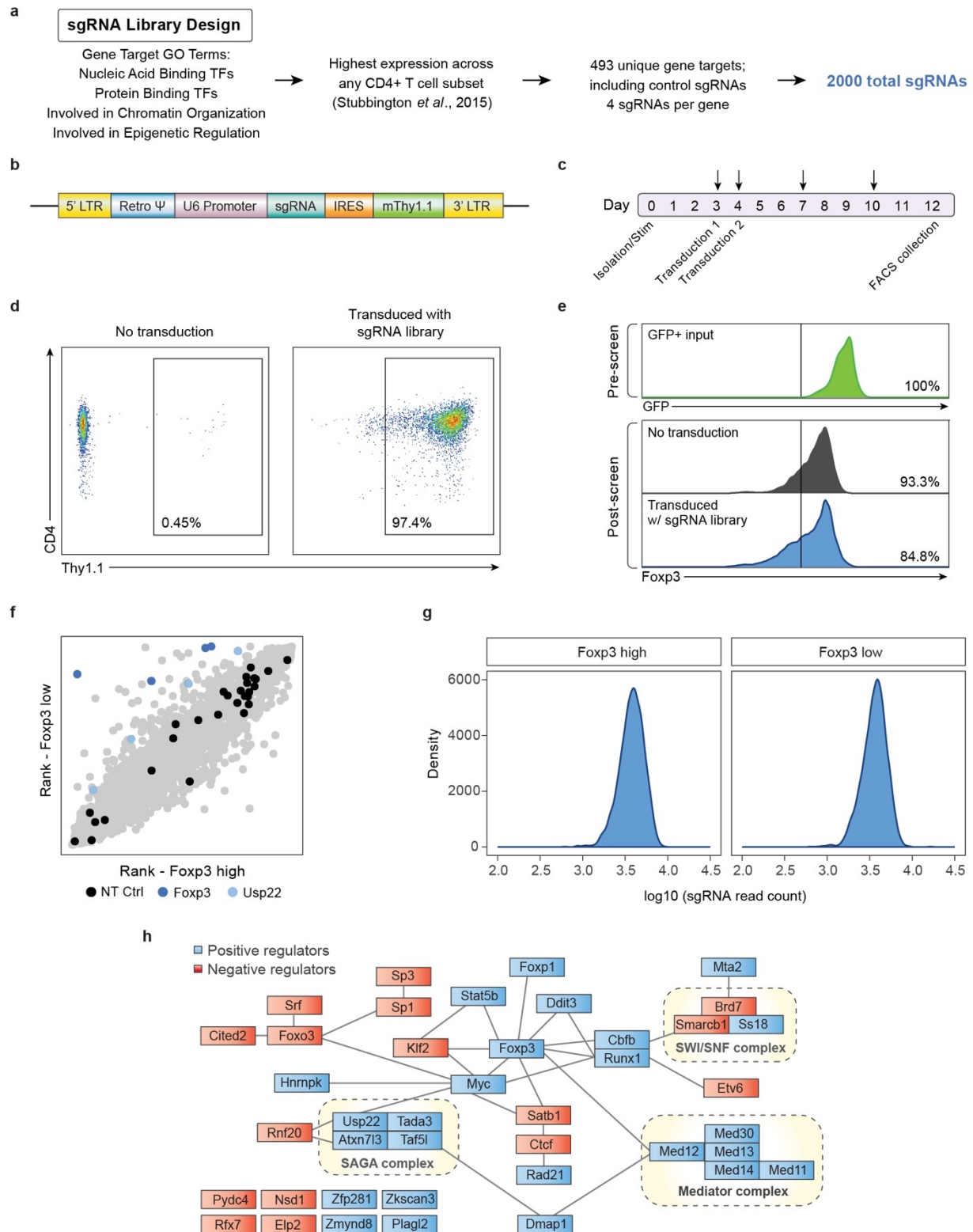
- a) Body weight differences between *Usp22*^{+/+}*Foxp3*^{YFP-Cre} WT or *Usp22*^{fl/fl}*Foxp3*^{YFP-Cre} KO littermate mice.
- b) Hematoxylin-and-eosin (H&E) staining of kidney, lung, colon and liver sections from 7-month-old *Usp22*^{+/+}*Foxp3*^{YFP-Cre} WT or *Usp22*^{fl/fl}*Foxp3*^{YFP-Cre} KO mice. Original magnification at 100x (fold).
- c) Body weight of Rag^{-/-} recipient mice over time after adoptive transfer of CD4⁺CD25⁻CD44^{lo}CD62^{hi} (CD45.1⁺) naïve T cells sorted from SJL mice alone or together with

CD4⁺YFP⁺ (CD45.2⁺) Treg cells from 9-week-old *Usp22*^{+/+}*Foxp3*^{YFP-Cre} WT or *Usp22*^{fl/fl}*Foxp3*^{YFP-Cre} KO mice, presented relative to weight at day 0.

- d) H&E staining of colon tissues from the Rag^{-/-} recipient mice shown in panel c, 7 weeks post-transfer. Original magnification at 100x.
- e) Clinical severity of EAE in *Usp22*^{+/+}*Foxp3*^{YFP-Cre} WT or *Usp22*^{fl/fl}*Foxp3*^{YFP-Cre} KO mice was monitored for 20 days post immunization with MOG peptide.
- f) EG7 lymphoma tumor volume in *Usp22*^{+/+}*Foxp3*^{YFP-Cre} WT or *Usp22*^{fl/fl}*Foxp3*^{YFP-Cre} KO mice. Mice were subcutaneously inoculated with 1x10⁶ EG7 cells. Tumor volume was measured every 1-2 days by scaling along 3 orthogonal axes (x, y, and z) and calculated as (xyz)/2.
- g) Representative flow cytometry analysis of the expression of CD44 and CD62L in both CD4⁺ and CD8⁺ T cells of spleen from *Usp22*^{+/+}*Foxp3*^{YFP-Cre} WT or *Usp22*^{fl/fl}*Foxp3*^{YFP-Cre} KO EG7 tumor-bearing mice.
- h) The frequency of effector T cells (CD44^{hi}CD62L^{lo}) from *Usp22*^{+/+}*Foxp3*^{YFP-Cre} WT or *Usp22*^{fl/fl}*Foxp3*^{YFP-Cre} KO EG7 tumor-bearing mice summarized.
- i) Statistical analysis of tumor-infiltrating lymphocyte (TIL) percentages from EG7-bearing *Usp22*^{+/+}*Foxp3*^{YFP-Cre} WT or *Usp22*^{fl/fl}*Foxp3*^{YFP-Cre} KO mice collected 19 days after tumor inoculation.
- j) Statistical analysis of tumor-infiltrating Treg percentages from EG7 tumor-bearing *Usp22*^{+/+}*Foxp3*^{YFP-Cre} WT or *Usp22*^{fl/fl}*Foxp3*^{YFP-Cre} KO mice collected 19 days after tumor inoculation.
- k) Foxp3 MFI of the CD4⁺Foxp3⁺ EG7 tumor-infiltrating Treg population in *Usp22*^{+/+}*Foxp3*^{YFP-Cre} WT or *Usp22*^{fl/fl}*Foxp3*^{YFP-Cre} KO mice summarized.

All data are presented as mean ±SEM. ns indicates no significant difference, *P < 0.05, **P < 0.01, ***P < 0.001, ****P < 0.0001.

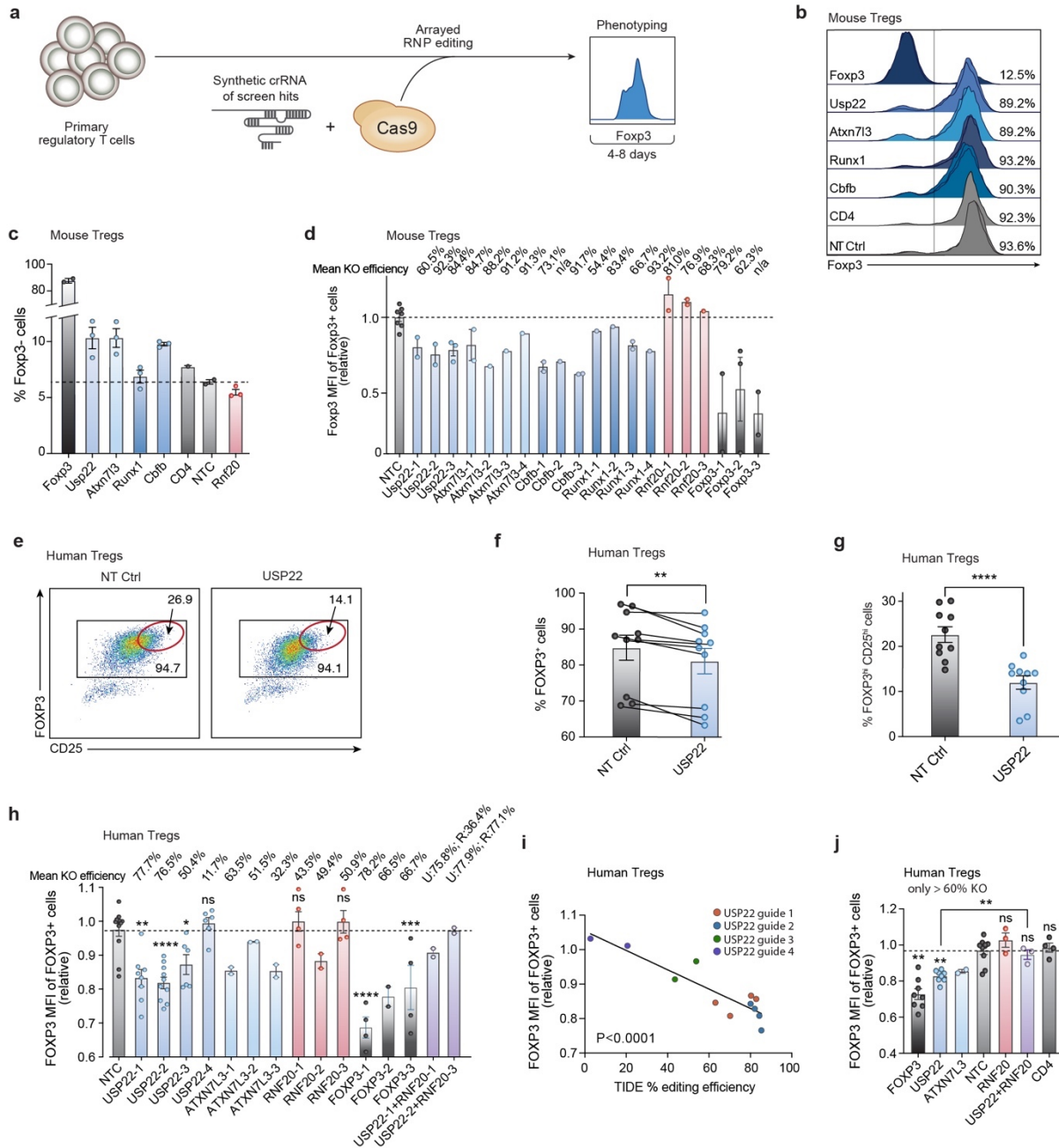
Figure 2.4. Design and quality control of targeted pooled CRISPR screen in primary mouse Tregs.



- a) Design strategy for selection of genes for unbiased targeted library of 493 targets, including 490 nuclear factors and 3 control targets (NT, GFP, and RFP). Genes were selected based on gene ontology (GO) annotation and then sub-selected based on highest expression across any CD4 T cell subset for a total of 2,000 sgRNAs.
- b) Diagram of MSCV expression vector with Thy1.1 reporter used for retroviral transduction of the sgRNA library.
- c) Detailed timeline schematic of the 12-day targeted screen pipeline. Arrows indicate when the cells were split, and media was replenished.
- d) Retroviral transduction efficiency of the targeted library in primary mouse Tregs shown by Thy1.1 surface expression measured by flow cytometry. The infection was scaled to achieve a high efficiency multiplicity of infection.
- e) Foxp3 expression from screen input, output and control cells measured by flow cytometry. Top: Foxp3 expression from input Foxp3⁺ purified Tregs as measured by GFP expression on Day 0. Middle: Foxp3 expression as measured by endogenous intracellular staining from control Tregs (not transduced with library) on Day 12. Bottom: Foxp3 expression as measured by endogenous intracellular staining from screen Tregs (transduced with library) on Day 12.
- f) Targeted screen (2,000 guides) shows that sgRNAs targeting Foxp3 and Usp22 were enriched in Foxp3 low cells (blue). Non-targeting control (NT Ctrl) sgRNAs were evenly distributed across the cell populations (black).
- g) Distribution of read counts after next generation sequencing of sgRNAs of sorted cell populations, Foxp3^{high} and Foxp3^{low}.
- h) Schematic of experimentally determined and predicted protein-protein interactions between top hits, 16 negative regulators (red) and 25 positive regulators (red), generated by STRING-db³⁹. Black lines connect interacting proteins and dotted lines outline selected known protein complexes.

All data are presented as mean \pm SEM. ns indicates no significant difference, *P < 0.05, **P < 0.01, ***P < 0.001, ****P < 0.0001.

Figure 2.5. Validation of Foxp3 modulators in primary mouse and human Tregs with Cas9 RNP electroporation.

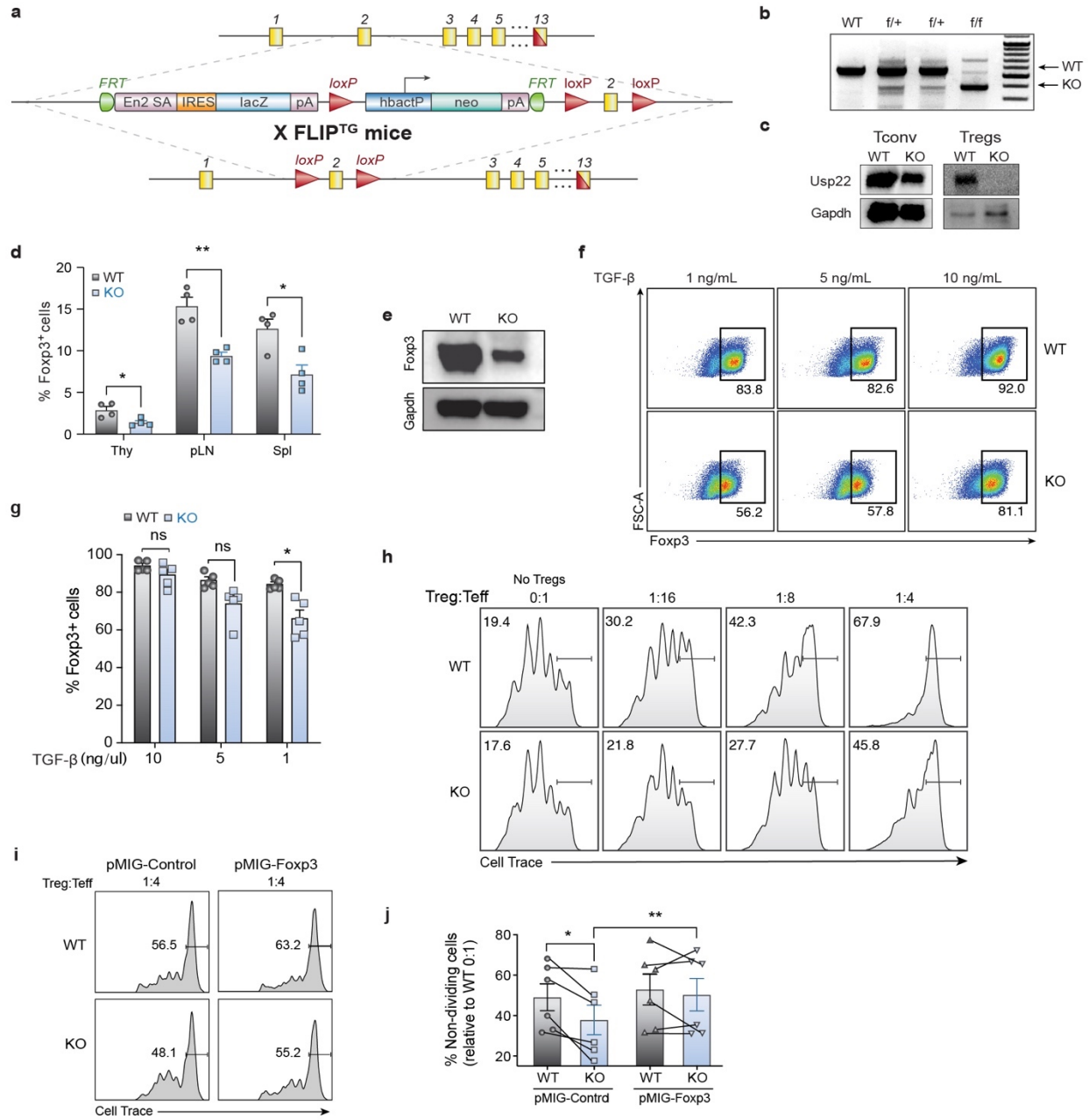


- Overview of orthogonal validation strategy using arrayed electroporation of Cas9 RNPs in Tregs.
- Foxp3 expression 4 days post-electroporation of Cas9 RNPs in mouse Tregs as measured by flow cytometry of top screen hits. Each row shows 3 histograms layered on top of one another (1-2 for controls) with each representing effects of independent gRNAs for each target gene. Percentages shown on the right depict the average frequency of Foxp3⁺ cells across gRNAs targeting each gene.

- c) Percentage of Foxp3⁻ cells of live, CD4⁺ cells 4 days post electroporation of Cas9 RNPs in mouse Tregs as measured by flow cytometry of top screen hits. Each data point represents an independent sgRNA for each target gene.
- d) Foxp3 MFI of Foxp3⁺ mouse Tregs for 3-4 distinct gRNAs targeting each gene paired with the mean KO efficiency (top) for each guide as determined by TIDE analysis.
- e) Representative flow plots depicting FOXP3 and CD25 expression 7 days post electroporation of Cas9 RNPs targeting USP22 or NT Ctrl in human Tregs. The subpopulation of cells with the highest expression of FOXP3 and CD25 (FOXP3^{hi}CD25^{hi}) is highlighted with a red gate.
- f) Percentage of FOXP3⁺ cells from human Tregs electroporated with Cas9 RNPs targeting USP22 or NT Ctrl in 10 biological replicates. Lines connect paired samples.
- g) Percentage of FOXP3^{hi}CD25^{hi} cells from human Tregs electroporated with Cas9 RNPs targeting USP22 or NT Ctrl in 10 biological replicates.
- h) FOXP3 MFI of human Tregs for 3-4 distinct gRNAs targeting each gene paired with the mean KO efficiency (top) for each guide as determined by TIDE analysis.
- i) Simple linear regression of FOXP3 MFI (y-axis) by percentage of editing efficiency determined by TIDE analysis (x-axis) for 4 gRNAs targeting USP22 in 2-4 biological donors.
- j) FOXP3 MFI of human Tregs electroporated with Cas9 RNPs with 2-3 distinct sgRNAs each in 2-4 biological donors; corresponding to panel h. Data points with less than 60% editing efficiency KO by TIDE analysis were excluded from the graph.

All data are presented as mean \pm SEM. ns indicates no significant difference, *P < 0.05, **P < 0.01, ***P < 0.001, ****P < 0.0001.

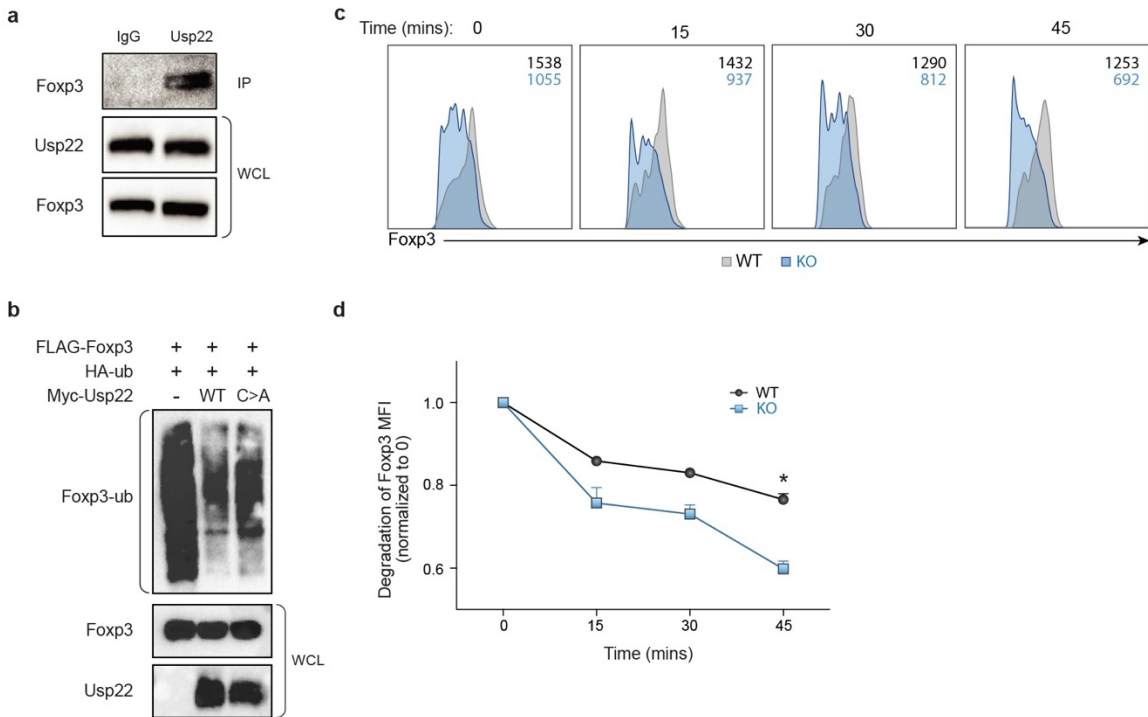
Figure 2.6. Design and validation of Treg-specific *Usp22* knockout mice.



- Diagram of the murine *Usp22* locus. Targeting vector contains IRES-lacZ and a neo cassette inserted into exon 2.
- Genotyping by PCR showed a 600-bp band for the wild-type allele and a 400-bp band for mutant allele, simultaneously in the homozygous floxed (*f/f*) mice.
- Western blot analysis of *Usp22* in CD4⁺CD25⁻ conventional T cells (Tconv) and CD4⁺CD25⁺ Treg cells isolated from *Usp22*^{+/+}*Foxp3*^{YFP-Cre} WT and *Usp22*^{f/f}*Foxp3*^{YFP-Cre} KO mice. Gapdh was used as a loading control.
- Statistical analysis of CD4⁺*Foxp3*⁺ Treg frequencies, corresponding to Figure 2c.

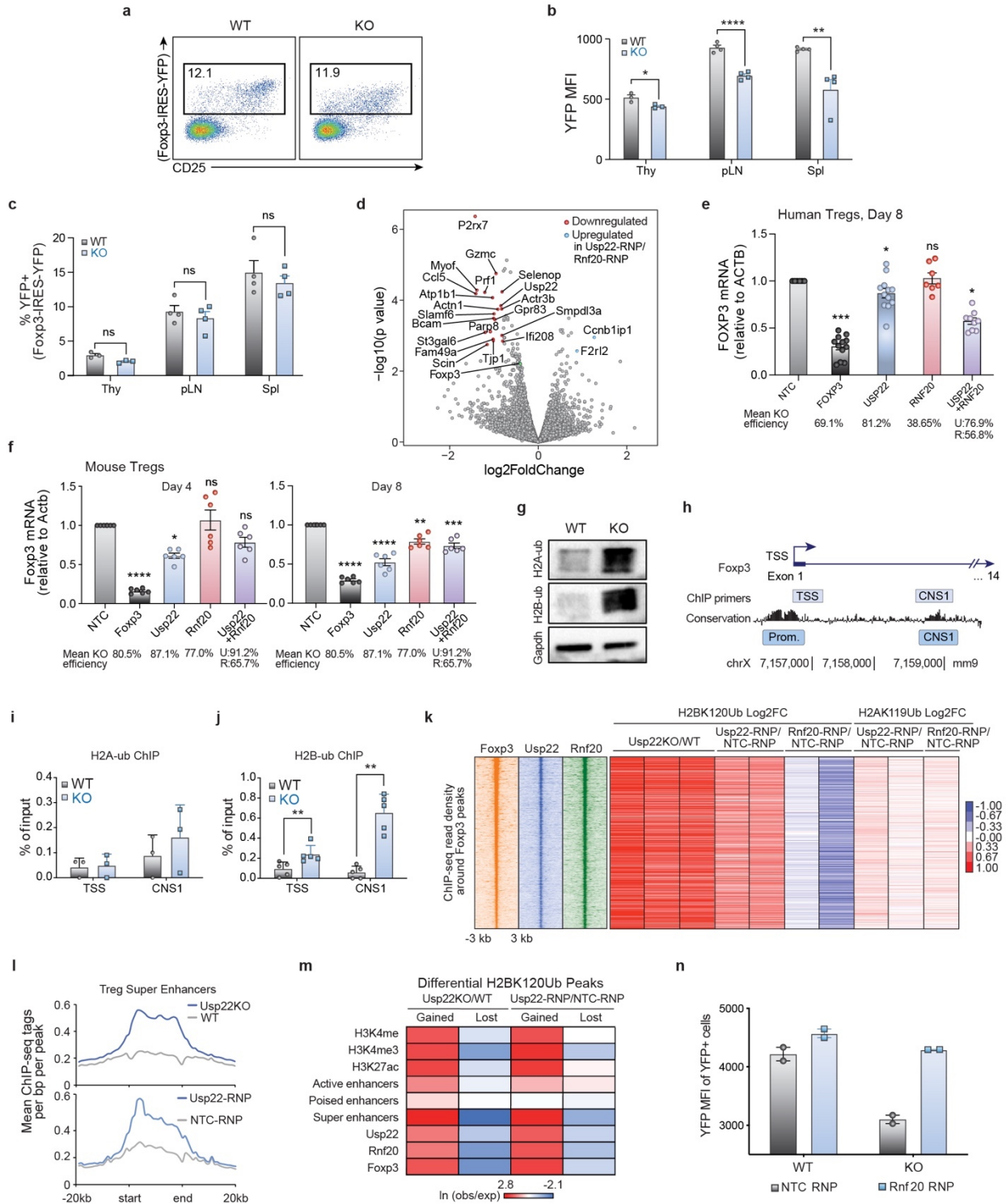
- e) Western blot analysis of Foxp3 protein level from Tregs isolated from spleen and LN of *Usp22^{+/+}Foxp3^{YFP-Cre}* WT or *Usp22^{fl/fl}Foxp3^{YFP-Cre}* KO mice. Gapdh was used as a loading control.
 - f) iTreg differentiation of naïve CD4⁺ T cells from *Usp22^{+/+}Foxp3^{YFP-Cre}* WT or *Usp22^{fl/fl}Foxp3^{YFP-Cre}* KO mice with titration of TGF-β (as indicated).
 - g) Summary of iTreg differentiation of naïve CD4⁺ T cells from *Usp22^{+/+}Foxp3^{YFP-Cre}* WT or *Usp22^{fl/fl}Foxp3^{YFP-Cre}* KO mice with titration of TGF-β (as indicated).
 - h) *In vitro* suppressive activity of Tregs assessed by the division of naïve CD4⁺CD25⁻ T cells. Naïve T cells were labeled with cytosolic cell proliferation dye and activated by anti-CD3 and antigen presenting cells (irradiated splenocytes from wild-type mice, depleted of CD3⁺ T cells), then co-cultured at various ratios (as indicated above) with YFP⁺ Treg cells sorted from 8-week-old *Usp22^{+/+}Foxp3^{YFP-Cre}* WT or *Usp22^{fl/fl}Foxp3^{YFP-Cre}* KO mice. Numbers indicate the percentage of non-dividing cells for each ratio.
 - i) *In vitro* suppressive activity of control (pMIG-Control) or Foxp3+ (pMIG-Foxp3) transduced YFP⁺ Tregs sorted from *Usp22^{+/+}Foxp3^{YFP-Cre}* WT or *Usp22^{fl/fl}Foxp3^{YFP-Cre}* KO mice. Naïve T cells were labeled with cytosolic cell proliferation dye and activated then co-cultured at 1:4 transduced YFP⁺ Treg cells to naïve T effectors (Teff). Numbers indicate the percentage of non-dividing cells for each ratio.
 - j) Summary data of *in vitro* suppression experiments represented as frequency of non-dividing cells relative to WT 0:1 No Treg control, corresponding to panel i. Lines connect paired samples.
- All data are presented as mean ±SEM. ns indicates no significant difference, *P < 0.05, **P < 0.01, ***P < 0.001, ****P < 0.0001.

Figure 2.7. Usp22 acts as deubiquitinase to control post-translational Foxp3 expression.



- a) Endogenous interaction of Usp22 and Foxp3 in murine iTreg cells from WT mice. Rabbit anti-Usp22 antibody was used to perform the immunoprecipitation and mouse anti-Foxp3 antibody was used to detect the bound Foxp3. Normal rabbit IgG was used as control. Whole cell lysates (WCL) were used as sample processing controls.
- b) Ubiquitination assay of Foxp3. HEK293 cells were co-transfected with Flag-Foxp3 and HA-ubiquitin (HA-ub) along with either Myc-empty vector, Myc-Usp22, or the catalytically inactive degradation mutant Myc-Usp22C185A (C>A), and then immunoprecipitated with anti-Flag and immunoblotted for HA-ubiquitin (Foxp3-ub). Whole cell lysates (WCL) were used as sample processing controls.
- c) Splenocytes isolated from *Usp22^{+/+}Foxp3^{YFP-Cre}* WT or *Usp22^{fl/fl}Foxp3^{YFP-Cre}* KO mice were treated with 200 μ g/ml cycloheximide (CHX) for the indicated time course. Inset numbers for each histogram indicate the MFI of Foxp3 in Tregs (black=WT, blue=KO).
- d) Foxp3 MFI from splenic CD4⁺CD25⁺Foxp3⁺ Treg population treated with 200 μ g/ml cycloheximide (CHX) for the indicated time course, n=3; corresponding to panel c. All data are presented as mean \pm SEM. ns indicates no significant difference, *P < 0.05, **P < 0.01, ***P < 0.001, ****P < 0.0001.

Figure 2.8. Usp22 regulates Foxp3 through transcriptional mechanisms.



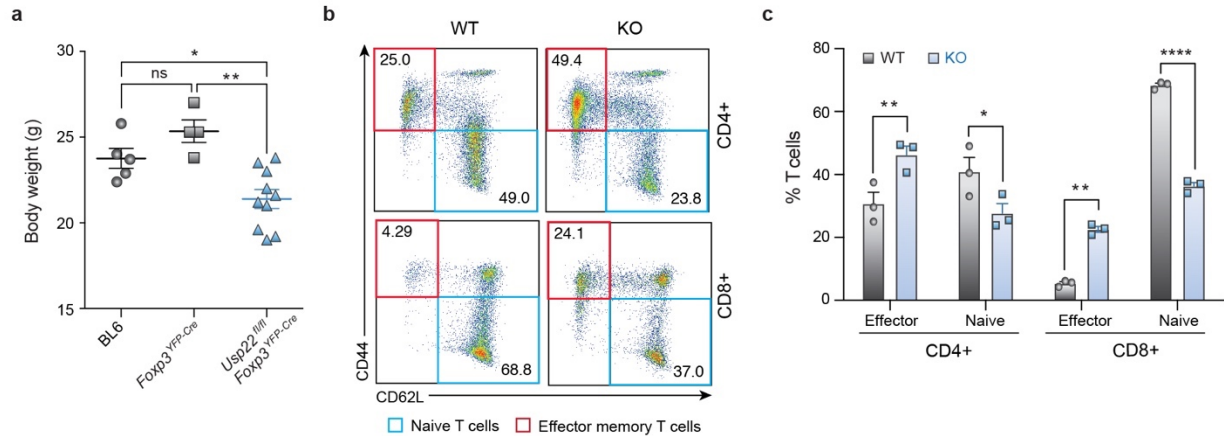
a) Representative flow cytometry analysis of the YFP⁺ Treg population (gated on CD4⁺ cells) from the spleen and lymph nodes of *Usp22*^{+/+}*Foxp3*^{YFP-Cre} WT or *Usp22*^{fl/fl}*Foxp3*^{YFP-Cre} KO mice.

- b) Statistical analysis of YFP MFI in CD4⁺YFP⁺ Tregs from the thymus (Thy), peripheral lymph nodes (pLN), and spleen (Spl) of *Usp22*^{+/+}*Foxp3*^{YFP-Cre} WT or *Usp22*^{fl/fl}*Foxp3*^{YFP-Cre} KO mice.
- c) Statistical analysis of CD4⁺YFP⁺ Treg frequencies in *Usp22*^{+/+}*Foxp3*^{YFP-Cre} WT or *Usp22*^{fl/fl}*Foxp3*^{YFP-Cre} KO mice, corresponding to panel b.
- d) Volcano plot for RNA sequencing of *Usp22* RNP KO Tregs vs *Rnf20* RNP KO murine Tregs. X-axis shows log₂FoldChange (LFC). Y-axis shows the -log₁₀ of the p-value as calculated by DESeq2. Genes downregulated in the *Usp22* RNP KO compared to *Rnf20* RNP KO are shown in red and genes upregulated are shown in blue defined by p-value <5e-3 and LFC > 0.8. *Foxp3* (shown in green) trended down but did not reach significance.
- e) qPCR analysis of *FOXP3* mRNA levels in human Tregs from 2 donors 8 days post-electroporation with Cas9 RNPs targeting *NTC*, *FOXP3*, *USP22*, *RNF20* or both *USP22* and *RNF20*. Normalized to the expression of β -ACTIN transcripts. Data are presented as mean \pm SEM and are representative of at least two independent experiments.
- f) qPCR analysis of *Foxp3* mRNA levels in mouse Tregs 4 and 8 days post-electroporation with Cas9 RNPs targeting *NTC*, *Foxp3*, *Usp22*, *Rnf20* or both *Usp22* and *Rnf20*. Normalized to the expression of β -actin transcripts.
- g) Western blot analysis of ubiquitinated histone 2A (H2AK119Ub; H2A-ub) and ubiquitinated histone 2B (H2BK120Ub; H2B-ub) from iTregs from *Usp22*^{+/+}*Foxp3*^{YFP-Cre} WT or *Usp22*^{fl/fl}*Foxp3*^{YFP-Cre} KO mice. *Gapdh* was used as a loading control.
- h) Schematic of *Foxp3* locus depicting PCR products used for ChIP-qPCR data shown in panel i and panel j.
- i) ChIP-qPCR data analysis for H2AK119Ub (H2A-ub) where primers amplified across the transcriptional start site (TSS) and the CNS1 enhancer region of the *Foxp3* locus. Data are normalized to the input and are presented as mean \pm SD.
- j) ChIP-qPCR data analysis for H2BK120Ub (H2B-ub) for PCR across the transcriptional start site (TSS) and across the CNS1 enhancer region of the *Foxp3* locus. Data are normalized to the input and are presented as mean \pm SD.
- k) Heatmap of ChIP-seq read density for *Foxp3*, *Usp22*, and *Rnf20* at sites bound by *Foxp3* (using previously published *Foxp3* ChIP data⁴⁰), ranked by highest to lowest *Foxp3* binding signal. The corresponding log₂ fold change (log₂fc) for either H2BK120Ub or H2AK119Ub upon *Usp22* or *Rnf20* deletion at these sites are plotted on the right, with each biological replicate shown as an individual column.
- l) Average ChIP-seq read density of H2BK120Ub at Treg super enhancers in control versus *Usp22*-deficient Tregs.
- m) Co-occurrence analysis showing the natural log of the ratio of the observed number of overlapping regions over the expected values for sites that either gain or lose H2BK120Ub in *Usp22*-deficient Tregs against publicly available histone modifications H3K4me, H3K4me3 and H3K27ac as well as enhancer classes, as described in the Methods.
- n) Analysis of reciprocal regulation of *Foxp3* by deubiquitinase *Usp22* and E3 ubiquitin ligase *Rnf20*. YFP MFI of Tregs sorted from *Usp22*^{+/+}*Foxp3*^{YFP-Cre} WT or

Usp22^{fl/fl}Foxp3^{YFP-Cre} KO mice and then electroporated with either NT control (NTC-RNP) or Rnf20 RNP, corresponding with Figure 2j where Foxp3 MFI from the same experiment is shown.

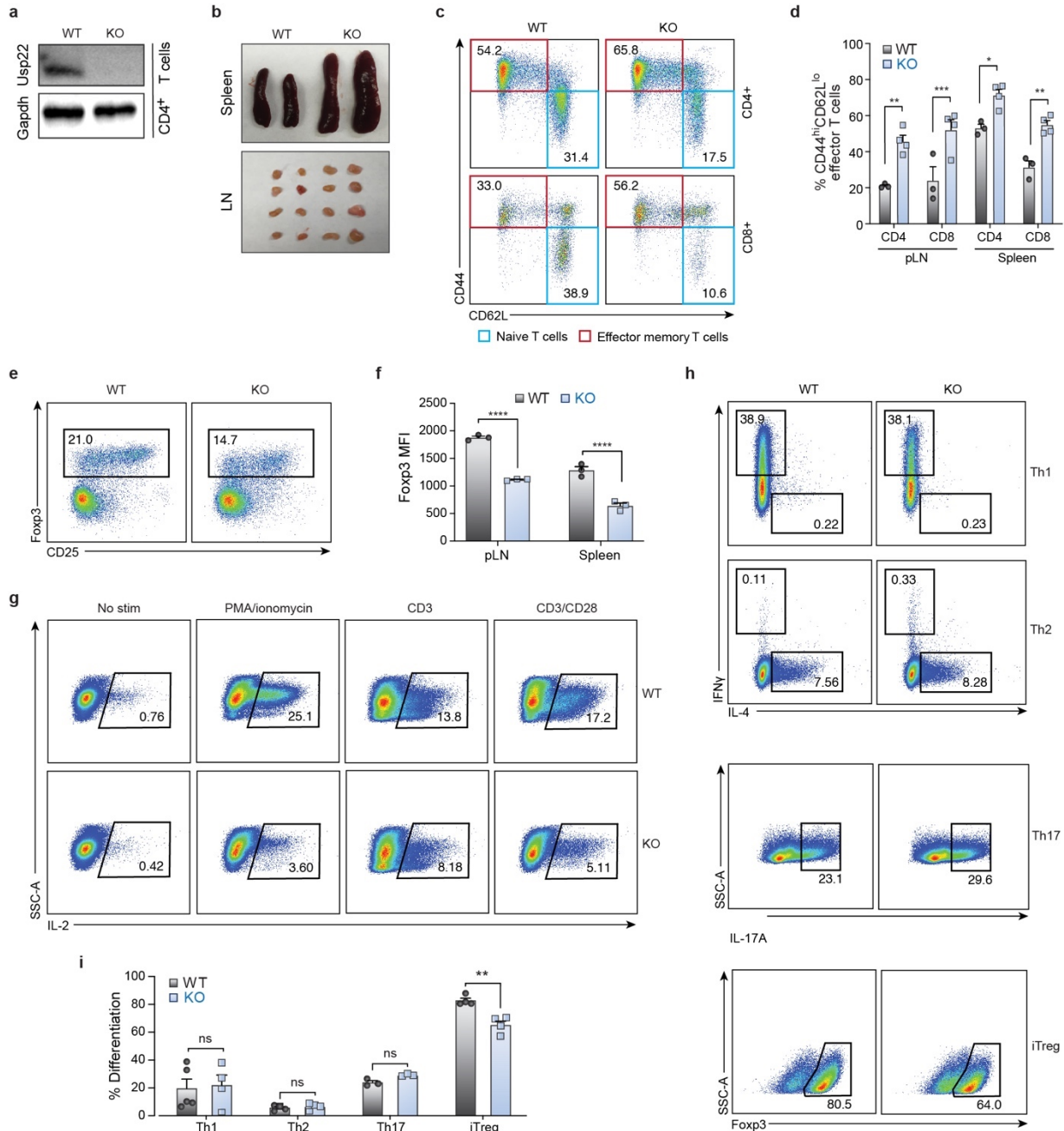
All data are presented as mean \pm SEM, unless otherwise stated. ns indicates no significant difference, *P < 0.05, **P < 0.01, ***P < 0.001, ****P < 0.0001.

Figure 2.9. Autoimmune inflammation in Treg-specific *Usp22* knockout mice.



- a) Body weight differences (in grams, g) between 8-week-old, sex-matched C57BL/6 WT (BL6), *Usp22^{+/+}Foxp3^{YFP-Cre}* WT or *Usp22^{fl/fl}Foxp3^{YFP-Cre}* KO mice.
- b) Representative flow cytometry analysis of CD44 and CD62L expression in splenic CD4⁺ and CD8⁺ T cells from aged 7-month-old *Usp22^{+/+}Foxp3^{YFP-Cre}* WT and *Usp22^{fl/fl}Foxp3^{YFP-Cre}* KO mice. Numbers in quadrants indicate percentage of each cell population.
- c) The frequency of splenic CD4⁺ and CD8⁺ effector T cells (CD44^{hi}CD62L^{lo}) and naïve T cells (CD44^{lo}CD62L^{hi}) of aged 7-month-old *Usp22^{+/+}Foxp3^{YFP-Cre}* WT and *Usp22^{fl/fl}Foxp3^{YFP-Cre}* KO mice summarized, corresponding to panel b.
- All data are presented as mean ±SEM. ns indicates no significant difference, *P < 0.05, **P < 0.01, ***P < 0.001, ****P < 0.0001.

Figure 2.10. T cell-specific ablation of *Usp22* resulted in decreased Foxp3 and increased T cell activation.

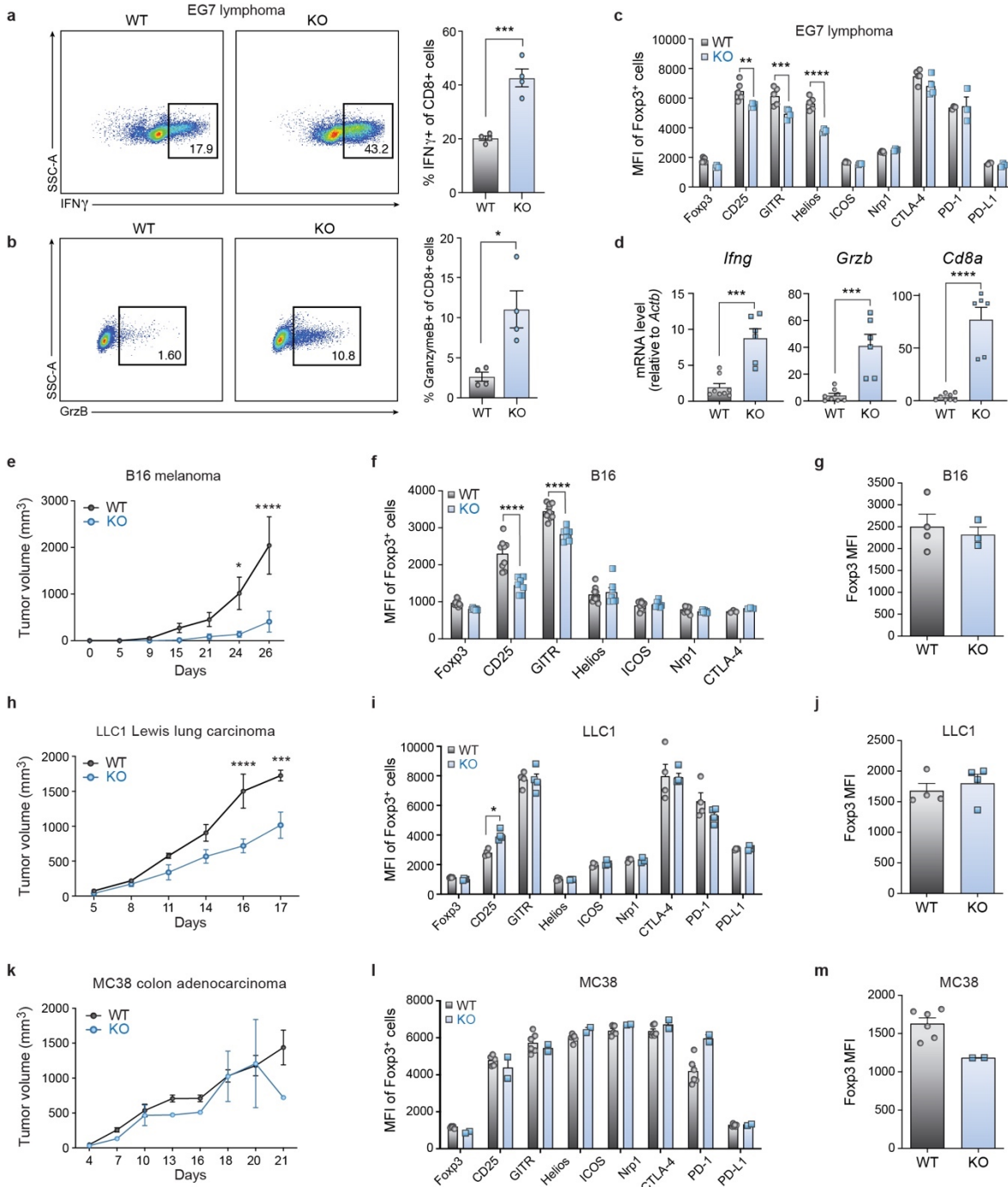


- a) Western blot analysis of *Usp22* protein levels in CD4⁺ T cells isolated from spleens of *Usp22^{fl/fl}Lck^{Cre}* KO and *Usp22^{+/+}Lck^{Cre}* WT mice. Gapdh was used as a loading control.
- b) Representative macroscopic images of spleens and peripheral lymph nodes (pLN) from 10-month-old *Usp22^{fl/fl}Lck^{Cre}* KO and *Usp22^{+/+}Lck^{Cre}* WT mice.

- c) Representative flow cytometry plots showing CD44 and CD62L expression in CD4⁺ and CD8⁺ T cells from spleens of 10-month-old *Usp22^{fl/fl}Lck^{Cre}* KO and *Usp22^{+/+}Lck^{Cre}* WT mice.
- d) Frequency of effector-memory T cells (CD44^{hi}CD62L^{lo}) in peripheral lymph nodes (pLN) and spleens from 10-month-old *Usp22^{fl/fl}Lck^{Cre}* KO and *Usp22^{+/+}Lck^{Cre}* WT mice.
- e) Representative flow cytometry plots showing the splenic CD4⁺Foxp3⁺ Treg population from 10-month-old *Usp22^{fl/fl}Lck^{Cre}* KO and *Usp22^{+/+}Lck^{Cre}* WT mice.
- f) Foxp3 MFI of the CD4⁺Foxp3⁺ Treg population in the spleen and pLN from 10-month-old *Usp22^{fl/fl}Lck^{Cre}* KO and *Usp22^{+/+}Lck^{Cre}* WT mice.
- g) IL-2 production by CD4⁺CD25⁻ T cells under various stimulation conditions (as indicated) for 3 days was assessed by flow cytometry in *Usp22^{fl/fl}Lck^{Cre}* KO and *Usp22^{+/+}Lck^{Cre}* WT mice. Although the dominant effect of *Usp22*-deficiency in T cells was increased T cell activation and lymphoproliferation, we found some evidence of impaired IL-2 production in conventional T cells.
- h) *Usp22*-deficiency in T cells led to a selective defect in iTreg differentiation. *In vitro* differentiation of CD4⁺ naïve T cells cultured under Th1, Th2, Th17 or sub-optimal TGF-β (1ng/mL) iTreg conditions from *Usp22^{fl/fl}Lck^{Cre}* KO and *Usp22^{+/+}Lck^{Cre}* WT mice was assessed by flow cytometry.
- i) Summary of *in vitro* differentiation experiments showing percent differentiation, corresponding to panel h.

All data are presented as mean ±SEM. ns indicates no significant difference, *P < 0.05, **P < 0.01, ***P < 0.001, ****P < 0.0001.

Figure 2.11. Tumor growth is inhibited in Treg-specific *Usp22* knockout mice in multiple cancer models.



a) Left: Representative flow cytometric analysis of splenic IFN γ in CD8 $^+$ T cells from EG7 tumor-bearing *Usp22* $^{+/+}$ *Foxp3* $^{YFP-Cre}$ WT or *Usp22* $^{fl/fl}$ *Foxp3* $^{YFP-Cre}$ KO. Right: Statistical analysis of IFN γ production by splenic CD8 $^+$ T cells from EG7 tumor-bearing *Usp22* $^{+/+}$ *Foxp3* $^{YFP-Cre}$ WT or *Usp22* $^{fl/fl}$ *Foxp3* $^{YFP-Cre}$ KO.

- b) Left: Representative flow cytometric analysis of splenic Granzyme B (GrzB) in CD8⁺ T cells from EG7 tumor-bearing *Usp22*^{+/+}*Foxp3*^{YFP-Cre} WT or *Usp22*^{fl/fl}*Foxp3*^{YFP-Cre} KO. Right: Statistical analysis of Granzyme B production by splenic CD8⁺ T cells from EG7 tumor-bearing *Usp22*^{+/+}*Foxp3*^{YFP-Cre} WT or *Usp22*^{fl/fl}*Foxp3*^{YFP-Cre} KO.
- c) The MFI of various Treg markers (as indicated) from splenic CD4⁺*Foxp3*⁺ Tregs from *Usp22*^{+/+}*Foxp3*^{YFP-Cre} WT or *Usp22*^{fl/fl}*Foxp3*^{YFP-Cre} KO EG7 tumor-bearing mice, assessed by flow cytometry.
- d) qPCR analysis of *Ifng*, *Gzmb* and *Cd8a* mRNA levels in the tumor tissue of *Usp22*^{+/+}*Foxp3*^{YFP-Cre} WT or *Usp22*^{fl/fl}*Foxp3*^{YFP-Cre} KO EG7 tumor-bearing mice.
- e) Tumor volumes from *Usp22*^{+/+}*Foxp3*^{YFP-Cre} WT or *Usp22*^{fl/fl}*Foxp3*^{YFP-Cre} KO mice subcutaneously inoculated with 5x10⁴ B16 melanoma cells. For e, h, k, tumor volumes were measured every 2-3 days by scaling along 3 orthogonal axes (x, y, and z) and calculated as (xyz)/2.
- f) The MFI of various Treg markers (as indicated) from splenic CD4⁺*Foxp3*⁺ Tregs in *Usp22*^{+/+}*Foxp3*^{YFP-Cre} WT or *Usp22*^{fl/fl}*Foxp3*^{YFP-Cre} KO B16 tumor-bearing mice, assessed by flow cytometry.
- g) *Foxp3* MFI of *Foxp3*⁺ cells from tumor-infiltrating Tregs in *Usp22*^{+/+}*Foxp3*^{YFP-Cre} WT or *Usp22*^{fl/fl}*Foxp3*^{YFP-Cre} KO B16 tumor-bearing mice.
- h) Tumor volumes from *Usp22*^{+/+}*Foxp3*^{YFP-Cre} WT or *Usp22*^{fl/fl}*Foxp3*^{YFP-Cre} KO mice subcutaneously inoculated with 1x10⁶ LLC1 Lewis lung carcinoma cells.
- i) The MFI of various Treg markers (as indicated) from splenic CD4⁺*Foxp3*⁺ Tregs in *Usp22*^{+/+}*Foxp3*^{YFP-Cre} WT or *Usp22*^{fl/fl}*Foxp3*^{YFP-Cre} KO LLC1 tumor-bearing mice, assessed by flow cytometry.
- j) *Foxp3* MFI of *Foxp3*⁺ cells from tumor-infiltrating Tregs in *Usp22*^{+/+}*Foxp3*^{YFP-Cre} WT or *Usp22*^{fl/fl}*Foxp3*^{YFP-Cre} KO LLC1 tumor-bearing mice.
- k) Tumor volumes from *Usp22*^{+/+}*Foxp3*^{YFP-Cre} WT or *Usp22*^{fl/fl}*Foxp3*^{YFP-Cre} KO mice subcutaneously inoculated with 1x10⁶ MC38 colon adenocarcinoma cells.
- l) The MFI of various Treg markers (as indicated) from splenic CD4⁺*Foxp3*⁺ Tregs in *Usp22*^{+/+}*Foxp3*^{YFP-Cre} WT or *Usp22*^{fl/fl}*Foxp3*^{YFP-Cre} KO MC38 tumor-bearing mice, assessed by flow cytometry.
- m) *Foxp3* MFI of *Foxp3*⁺ cells from tumor-infiltrating Tregs in *Usp22*^{+/+}*Foxp3*^{YFP-Cre} WT or *Usp22*^{fl/fl}*Foxp3*^{YFP-Cre} KO MC38 tumor-bearing mice.

All data are presented as mean ±SEM. ns indicates no significant difference, *P < 0.05, **P < 0.01, ***P < 0.001, ****P < 0.0001.

Tables

Table 2.1. Top 30 gene level hits from screen data.

id	nu m	neg s core	neg p- value	neg f dr	neg r ank	neg goo dsgrna	neg lfc	pos sc ore	pos p- value	pos f dr	pos r ank	pos goo dsgrna	pos lfc
Foxp 3	4	1	1	0.999 995	493	0	1.34 25	3.61E- 09	4.97E- 06	0.000 817	1	4	1.34 25
Usp 22	4	1	1	0.999 995	492	0	0.36 66	6.37E- 07	4.97E- 06	0.000 817	2	4	0.36 66
Cbfb	4	0.998 99	0.9988 6	0.999 995	488	0	0.71 208	6.43E- 06	4.97E- 06	0.000 817	3	4	0.71 208
Run x1	4	0.816 78	0.8172 9	0.999 995	401	1	0.37 272	4.63E- 05	0.0001 9389	0.019 118	4	3	0.37 272
Myc	4	0.999 95	0.9999 4	0.999 995	491	0	0.38 282	4.80E- 05	0.0001 9389	0.019 118	5	4	0.38 282
Ss18	4	0.960 17	0.9603	0.999 995	463	0	0.32 901	6.70E- 05	0.0002 7344	0.022 467	6	3	0.32 901
Med 30	4	0.632 22	0.6843 1	0.999 995	331	1	0.35 826	0.0001 5658	0.0006 115	0.040 033	7	3	0.35 826
Atxn 7l3	4	0.992 8	0.9929 5	0.999 995	480	0	0.46 354	0.0001 6422	0.0006 5127	0.040 033	8	4	0.46 354
Med 12	4	0.990 12	0.9904 8	0.999 995	478	0	0.33 721	0.0001 8536	0.0007 3082	0.040 033	9	4	0.33 721
Hnrn pk	4	0.999 74	0.9997 2	0.999 995	490	0	0.25 204	0.0002 622	0.0009 6945	0.047 794	10	4	0.25 204
Zfp2 81	4	0.999 58	0.9996 2	0.999 995	489	0	0.28 02	0.0004 2109	0.0015 561	0.069 742	11	4	0.28 02
Taf5l	4	0.954 93	0.9552 6	0.999 995	460	0	0.30 566	0.0007 3703	0.0027 89	0.114 583	12	3	0.30 566
Ddit 3	4	0.998 97	0.9988 5	0.999 995	487	0	0.16 312	0.0010 324	0.0038 828	0.138 831	13	4	0.16 312
Zmy nd8	4	0.996 53	0.9965 7	0.999 995	483	0	0.25 309	0.0010 568	0.0039 424	0.138 831	14	4	0.25 309
Med 14	4	0.730 89	0.7468	0.999 995	360	1	0.15 551	0.0011 953	0.0044 993	0.147 876	15	2	0.15 551
Rad 21	4	0.998 17	0.9981 1	0.999 995	486	0	0.16 141	0.0018 272	0.0065 774	0.190 223	16	4	0.16 141
Dma p1	4	0.988 74	0.9891 1	0.999 995	476	0	0.21 613	0.0019 075	0.0068 558	0.190 223	17	4	0.21 613
Med 11	4	0.994 51	0.9945 3	0.999 995	481	0	0.31 583	0.0019 501	0.0069 453	0.190 223	18	4	0.31 583
Zksc an3	4	0.997 81	0.9977 6	0.999 995	485	0	0.13 156	0.0021 869	0.0078 501	0.203 689	19	4	0.13 156
Foxp 1	4	0.997 07	0.9970 5	0.999 995	484	0	0.16 301	0.0029 347	0.0104 65	0.257 966	20	4	0.16 301
Stat 5b	4	0.558 26	0.6465 1	0.999 995	312	1	0.24 658	0.0051 143	0.0177 63	0.402 741	21	3	0.24 658
Med 13	4	0.994 82	0.9948 6	0.999 995	482	0	0.15 299	0.0051 78	0.0179 72	0.402 741	22	4	0.15 299
Plagl 2	4	0.888 19	0.8884	0.999 995	430	0	0.18 785	0.0055 238	0.0190 66	0.408 674	23	3	0.18 785
Tada 3	4	0.940 33	0.9411 9	0.999 995	453	0	0.20 472	0.0062 52	0.0213 73	0.439 032	24	3	0.20 472
Mta2	4	0.992 6	0.9928	0.999 995	479	0	0.12 335	0.0073 952	0.0251 91	0.496 765	25	4	0.12 335
Ceb pz	4	0.328 46	0.4735 4	0.999 995	216	1	0.15 394	0.0081 261	0.0275 08	0.521 587	26	2	0.15 394
Creb zf	4	0.913 22	0.9143 5	0.999 995	436	0	0.20 764	0.0087 668	0.0296 95	0.542 211	27	3	0.20 764
Per1	4	0.913 86	0.9149 4	0.999 995	437	0	0.19 095	0.0092 773	0.0311 87	0.549 107	28	3	0.19 095
Nac a	4	0.962 26	0.9624 2	0.999 995	465	0	0.19 788	0.0098 853	0.0330 36	0.561 613	29	3	0.19 788
Sma d4	4	0.989 48	0.9897 2	0.999 995	477	0	0.10 17	0.0105 19	0.0352 14	0.571 869	30	4	0.10 17

Table 2.2. List of primers

Primer_name	Sequence
Primers used for Pooled sgRNA Library Design and Construction	
MSCV Bsgl-Gib Fwd	CTTGTGCAGTTTTGTACGTCTCTGTTTTAGAGCTAGAAATAGC
MSCV Bsgl-Gib Rev	GTGTGTGCAGTTACAACCGTCTCCGGTGTTCGTCCTTTCCAC
Lenti-sgRNA ExcFod Bsgl Fwd	CGAAACACCGGAGACGGTTGTAAGTGCACACACAAAATACAC ATGC
Lenti-sgRNA ExcFod Bsgl Rev	CTAGCTCTAAAACAGAGACGTACAAAAGTGCACAAGAAGC
sgRNA Gib Lib Fwd (35)	GGCTTTATATATCTTGTGGAAAGGACGAAACACCG
sgRNA Gib Lib Rev (38)	CTAGCCTTATTTTAACTTGCTATTTCTAGCTCTAAAAC
Primers used for Preparation of Genomic DNA for Next Generation Sequencing	
PCR-SetA 3' common primer p7	CAAGCAGAAGACGGCATAACGAGATGGGTCGCTACAGACGTTG TTTG
PCR-SetA 5' index primer p5	AATGATACGGCGACCACCGAGATCTACACGATCGGAAGAGCA CACGTCTGAACTCCAGTCACCTTGTAGGACTATCATATGCTTA CCGTAAC
Index 3- PCR-SetA 5' index	AATGATACGGCGACCACCGAGATCTACACGATCGGAAGAGCA CACGTCTGAACTCCAGTCACAGTTCCGGACTATCATATGCTTA CCGTAAC
5' custom seq primer MSCVscreen	TTCGATTTCTTGGCTTTATATATCTTGTGGAAAGGACGAAACAC CG
Primers used for real-time qPCR (Figure 2.2f)	
Foxp3 Forward	GGCCCTTCTCCAGGACAGA
Foxp3 Reverse	GCTGATCATGGCTGGGTTGT
ChIP-qPCR Primers	
	(Takaki et al., 2008)
Primer 1 Fwd	cta gaa acc atg ctg caa aga c
Primer 1 Rev	gta ctc att ttc tca ggg tcc atg g
Primer 2 Fwd	cgc agc tgc cag atc ttg aat ac
Primer 2 Rev	cac tcc cgt ttg caa agg ttt agg
Primer 5 Fwd	cct ttt acc tct gtg gtg agg g
Primer 5 Rev	tat acc gag aag aaa aac cac ggc g
Primer 6 Fwd (TSS)	gat aat gtg gca gtt tcc cac aag c

Primer_name	Sequence
Primer 6 Rev (TSS)	ttt ttg ccc ctg tct aag gac caa c
Primer 10 Fwd (CNS1)	cag gct gac ctc aaa ctc aca aag
Primer 10 Rev (CNS1)	cat acc cac act ttt gac ctc tgc
Primer 11 Fwd	gtg ggc tat cta cgc agt cac tt
Primer 11 Rev	gag aca gtg aga gca gtt tag agg
Primer 12 Fwd	ctc cat aag att tac ccc agc cac
Primer 12 Rev	cat gct atg gtt atg gac tgg atc c
Primer 15 Fwd	caa tat cca tga ggc ctg cct aat ac
Primer 15 Rev	ctt ggc cag att ttt ctg cca ttg ac
Taqman Primer Probes used for real-time qPCR (Extended Data Figure 5)	
Mouse Actb Endogenous Control (VIC/MGB probe, primer limited) - ThermoFisher Cat# 4352341E	
Mouse Foxp3 Mm00475162_m1 (FAM/MGB probe) - Taqman, ThermoFisher Cat# 4331182	
Human ACTB Hs01060665_g1 (VIC/MGB probe, primer limited) - Taqman, ThermoFisher Cat# 4448484	
Human FOXP3 Hs01085834_m1 (FAM/MGB probe) - Taqman, ThermoFisher Cat# 4331182	
Primers used for real-time qPCR (Extended Data Figure 8))	
IFNy Forward	TGAACGCTACACACTGCATCT
IFNy Reverse	CACCATCCTTTTGCCAGTTCC
Grzb Forward	CATGCTGCTAAAGCTGAAGAGT
Grzb Reverse	GGACTCACACTCCCGATCCT
CD8 Forward	GTCCTTCTACAACACTGCCCC
CD8 Reverse	CTCTCCTCCGCACACAGTAAA
b-Actin Forward	AGATCAAGATCATTGCTCCTCCT
b-Actin Reverse	ACGCAGCTCAGTAACAGTCC

Table 2.3. List of crRNA

Species	Guide_name	Sequence
Mouse	mCD4 KO	CCTGGAAGTTCTCTGACCAG
Mouse	mFoxp3-1	CATACCTGATGCATGAAGTG
Mouse	mFoxp3-2	TCTACCCACAGGGATCAATG
Mouse	mFoxp3-3	AGGTCGGGACCTGCGAAGTG
Mouse	mFoxp3-4	GCAAGAGCTCTTGTCCATTG
Mouse	mUsp22-1	GCCATCGACCTGATGTACGG
Mouse	mUsp22-2	TTGACCAGATCTTTACGGGT
Mouse	mUsp22-3	TGCGTGGACTGATCAACCTG
Mouse	mUsp22-4	TGGGGCTCTGCATCTCACAG
Mouse	mAtxn7l3-1	GCAGCCGAATCGCCAACCGT
Mouse	mAtxn7l3-2	TGTCCAAAGATGTCCAACCC
Mouse	mAtxn7l3-3	TCTACTCACCTTAAAAGGAT
Mouse	mAtxn7l3-4	GTACACCGGGCTGTTAAGTG
Mouse	mRnf20-1	CAATCTGGGACACAGCACGG
Mouse	mRnf20-2	AAACGTTATGATCTGGACCA
Mouse	mRnf20-3	TAGCAGAAATGCTAGATCAG
Mouse	mRnf20-4	GCTATAAAGTATATGGAGCG
Mouse	mRunx1-1	TGCGCACTAGCTCGCCAGGG
Mouse	mRunx1-2	CGGTCCCTACACTAGGACAT
Mouse	mRunx1-3	AGAACTGAGAAATGCTACCG
Mouse	mRunx1-4	TTGTGGCGGATTTGTAAAGA
Mouse	mCbfb-1	GCCTTGCAGATTAAGTACAC
Mouse	mCbfb-2	AACCCATACCATCCAATCTG
Mouse	mCbfb-3	CGATCTCCGAGCGACCGTCG
Mouse	mCbfb-4	AAGTCGACATATTCCCGGCT
Mouse/Human	NTC-1	GCGACTAGTACGCGTAGGTT
Mouse/Human	NTC-2	TATGTACCCGTTGTACGCGC
Mouse/Human	NTC-3	GGTTCTTGACTACCGTAATT
Human	OS_1_USP22_B_KO	TGGGGCTCTGCATCTCACAG
Human	OS_2_USP22_KO	CAACTTATACGGGATGTGAG
Human	OS_3_USP22_KO	CATGGAAATAATCGCCAAGG
Human	OS_4_USP22_B_KO	GCCATTGATCTGATGTACGG
Human	OS_14_Foxp3_B_KO	CCCACCCACAGGGATCAACG
Human	OS_15_Foxp3_B_KO	CCTACTTAGGCACTGCCAGG
Human	OS_16_Foxp3_KS_KO	TCATGGCTGGGCTCTCCAGG
Human	OS_17_Foxp3_KO	CTTGAGGGAGAAGACCCAG
Human	JCg130: hATXN7L3.1.AA	GTACACCGGGCTGTCAAGTG

Species	Guide_name	Sequence
Human	JCg131: hATXN7L3.1.AB	AATGACAACGACTGGTCCTA
Human	JCg132: hATXN7L3.1.AC	TAATGACTTGGATCTTCGAG
Human	JCg133: hRNF20.1.AA	TATTGATTGTCAACCGATAC
Human	JCg134: hRNF20.1.AB	CAATCTGGGACACGGCTCGG
Human	JCg135: hRNF20.1.AC	CATCCTTAAACGTTATGATC
Human	OS_5: Human_CD4_B_KO	AGTGCAATGTAGGAGTCCAA

Table 2.4. List of Antibodies

Application	Target	Clone	Fluorophore	Vendor	Catalog Number
Flow Cytometry Antibodies					
Viability Dye	dead cells	N/A	Brilliant Violet 510	Tonbo	13-0870-T100
Viability Dye	dead cells	N/A	Alexa Fluor 506	eBioscience	65-0866-14
Mouse T Cell Surface Staining	CD90.1 (Thy1.1)	HIS51	APC	eBioscience	17-0900-82
Mouse T Cell Surface Staining	CD3e	145-2C11	PE	Biolegend	100307
Mouse T Cell Surface Staining	CD3e	17A2	PE-Cy7	Biolegend	100219
Mouse T Cell Surface Staining	CD3e	145-2C11	APC	Biolegend	100311
Mouse T Cell Surface Staining	CD4	GK1.5	Pacific Blue	BioLegend	100428
Mouse T Cell Surface Staining	CD4	GK1.5	PerCP-Cy5.5	Biolegend	100433
Mouse T Cell Surface Staining	CD4	GK1.5	APC Cy7	Biolegend	100413
Mouse T Cell Surface Staining	CD4	GK1.5	PE-Cy7	Biolegend	100421
Mouse T Cell Surface Staining	CD8a	53-6.7	Pacific Blue	Biolegend	100725
Mouse T Cell Surface Staining	CD25	PC61	APC	BioLegend	102012
Mouse T Cell Surface Staining	CD25	PC61	PE-Cy7	Biolegend	102016
Mouse T Cell Surface Staining	CD25	PC61	PE	Biolegend	102008
Mouse T Cell Surface Staining	CD44	IM7	PE-Cy7	Biolegend	103030
Mouse T Cell Surface Staining	CD44	IM7	APC	Biolegend	103011
Mouse T Cell Surface Staining	CD62L	MEL-14	APC	BioLegend	104412
Mouse T Cell Surface Staining	CD62L	MEL-14	PE	ebioscience	12-0621-82
Mouse T Cell Surface Staining	CD357 (GITR)	DTA-1	PerCP-Cy5.5	BioLegend	126315
Mouse T Cell Surface Staining	CD357 (GITR)	DTA-1	PE	BioLegend	126309
Mouse T Cell Surface Staining	CD128 (ICOS)	7E.17G9	PE	ebioscience	12-9942-81
Mouse T Cell Surface Staining	CD279 (PD-1)	29F.1A12	PE	BioLegend	135205
Mouse T Cell Surface Staining	CD274 (PD-L1)	10F.9G2	PE	BioLegend	124308
Mouse T Cell Surface Staining	CD103	2E7	PE	eBioscience	12-1031-82

Application	Target	Clone	Fluorophore	Vendor	Catalog Number
Mouse T Cell Intracellular Staining	Foxp3	FJK-16s	FITC	eBioscience	11-5773-82
Mouse T Cell Intracellular Staining	Foxp3	FJK-16s	PE	eBioscience	12-5773-82
Mouse T Cell Intracellular Staining	Usp22	C-3	Alexa Fluor 647	Santa Cruz Bio	sc-390585
Mouse T Cell Intracellular Staining	IL-2	JES6-5H4	APC	eBioscience	17-7021-81
Mouse T Cell Intracellular Staining	IFN-γ	XMG1.2	FITC	BioLegend	505806
Mouse T Cell Intracellular Staining	IL-4	11B11	APC	BioLegend	504105
Mouse T Cell Intracellular Staining	IL-17A	TC11-18H10.1	APC	BioLegend	506915
Mouse T Cell Intracellular Staining	Granzyme B	GB11	FITC	BioLegend	515403
Mouse T Cell Intracellular Staining	Helios	22F6	APC	BioLegend	137221
Mouse T Cell Intracellular Staining	CD152 (CTLA-4)	UC10-4B9	APC	BioLegend	106309
Mouse T Cell Intracellular Staining	CD152 (CTLA-4)	UC10-4B9	PE-Cy7	BioLegend	106313
Mouse T Cell Intracellular Staining	CD304 (Neuropilin-1)	3E12	APC	BioLegend	145205
Human T Cell Surface Staining	CD4	SK3	PerCP	Tonbo	67-0047-T500
Human T Cell Surface Staining	CD25	BC96	APC	Tonbo	20-0259-T100
Human T Cell Surface Staining	CD127	hIL-7R-M21	PE	BD	557938
Human T Cell Surface Staining	CD25	M-A251	PE-Cy7	BD	557741
Human T Cell Intracellular Staining	FOXP3	206D	Alexa Fluor 488	BioLegend	320112
Human T Cell Intracellular Staining	CD152 (CTLA4)	L3D10	APC	BioLegend	349908
Human T Cell Intracellular Staining	IFN-γ	B27	V450	BD	560371
Human T Cell Intracellular Staining	Helios	22F6	PerCP/Cy5.5	BioLegend	137230
Human T Cell Intracellular Staining	IL-2	MQ1-17H12	Brilliant Violet 650	BioLegend	500334
Human T Cell Intracellular Staining	IL-4	MP4-25D2	APC/Cy7	BioLegend	5000834
Human T Cell Intracellular Staining	IL-10	JES3-9D7	PE	BD	554498
Human T Cell Intracellular Staining	IL-17A	BL168	Alexa Fluor 700	BioLegend	512318

Target (Vendor, Catalog)					
Western Blot Antibodies					
HRP-conjugated Myc (Santa Cruz, Cat# 2040S)					
HRP-conjugated HA (Santa Cruz, Cat# 14031S)					
HRP-conjugated FLAG (Sigma, Cat# A8592)					
anti-GAPDH (Sigma, Cat# G9545)					
anti-Usp22 (Santa Cruz, Cat# sc-390585)					
anti-Foxp3 (eBioscience, Cat# 11-5773-82)					
Co-IP Antibodies					
anti-FLAG (Sigma, Cat# A8592)					
anti-Usp22 (Novus Biologicals, Cat# NBP1-49644)					
ChIP Antibodies					
rabbit anti-IgG (Cell Signaling, Cat# 2729)					
rabbit anti-USP22 (Abcam, ab195289)					
ub-Histone H2A Lys119 (Cell Signaling, Cat# 8204S)					
ub-Histone H2B Lys120 (Cell Signaling, Cat# 5546P)					
RNF20 Novus Biologicals, Cat# NB100-2242					

CHAPTER 3: METHODS

Mice for screen and RNP validation

B6 *Foxp3^{GFP-Cre}* mice⁴¹ were crossed with B6 *Rosa26^{LSL-RFP}* reporter mice⁴² as previously described⁴³ to generate the Foxp3 fate reporter mice. These mice were then crossed to B6 constitutive Cas9-expressing mice⁹ to generate the *Foxp3^{GFP-Cre}Rosa26^{LSL-RFP}Cas9* mice used for the CRISPR screen. For the arrayed validation experiments, B6 *Foxp3^{EGFP}* knock-in mice⁴⁴ that were obtained from Jackson Laboratories (Strain No. 006772) were used. These mice were maintained in the UCSF specific-pathogen-free animal facility in accordance with guidelines established by the Institutional Animal Care and Use Committee and Laboratory Animal Resource Center.

Isolation and culture of primary mouse Tregs for screen and validation

Spleens and peripheral lymph nodes were harvested from mice and dissociated in 1x PBS with 2% FBS and 1 mM EDTA. The mixture was then passed through a 70- μ m filter. CD4⁺ T cells were isolated using the CD4⁺ Negative Selection Kit (StemCell Technologies, Cat# 19752) followed by fluorescence-activated cell sorting. For the prescreen sort, Tregs were gated on lymphocytes, live cells, CD4⁺, CD62L⁺, RFP⁺, Foxp3-GFP⁺ cells. For the arrayed validation experiments, Tregs were gated on lymphocytes, live cells, CD4⁺, Foxp3-GFP⁺ cells. Sorted Tregs were cultured in complete DMEM, 10% FBS, 1% pen/strep + 2000U hIL-2 in 24 well plates at 1 million cells/mL. Tregs were stimulated using CD3/CD28 Mouse T-Activator Dynabeads (Thermo Fisher, Cat# 11456D) at a ratio of 3:1 beads to cells for 48 hours. Cells were split and media was refreshed every 2-3 days.

Pooled sgRNA library design and construction

For the cloning of the targeted library, we followed the custom sgRNA library cloning protocol as previously described⁴⁵. We utilized a MSCV-U6-sgRNA-IRES-Thy1.1 backbone (gifted from the Bluestone Lab). To optimize this plasmid for cloning the library, we first replaced the sgRNA with a 1.9kb stuffer derived from the lentiGuide-Puro plasmid (Addgene, plasmid# 52963) with flanking BsgI cut sites. This stuffer was excised using the BsgI restriction enzyme (NEB, Cat# R0559) and the linear backbone was gel purified (Qiagen, Cat# 28706). We designed a targeted library to include all genes matching Gene Ontology for “Nucleic Acid Binding Transcription Factors”, “Protein Binding Transcription Factors”, "Involved in Chromatin Organization" and "Involved in Epigenetic Regulation." Genes were then selected based on those that have the highest expression levels across any mouse CD4 T cell subset as defined by Stubbington *et al*⁴⁶. In total, we included 489 targets with 4 guides per gene, GFP and RFP controls with 8 guides for each, and 28 non-targeting controls. Guides were subsetting from the Brie sgRNA library¹³, and the pooled oligo library was ordered from Twist Bioscience (San Francisco, CA) to match the vector backbone. Oligos were PCR amplified and cloned into the modified MSCV backbone by Gibson assembly as described by Joung *et al*⁴⁵. The library was amplified using Endura ElectroCompetent Cells following the manufacturer’s protocol (Endura, Cat# 60242-1). All primer sequences are listed in **Table 2**.

Retrovirus production

Platinum-E (Plat-E) Retroviral Packaging cells (Cell Biolabs, Inc., Cat# RV-101) were seeded at 10 million cells in 15 cm poly-L-Lysine coated dishes 16 hours prior to

transfection and cultured in complete DMEM, 10% FBS, 1% pen/strep, 1 µg/mL puromycin and 10 µg/mL blasticidin. Immediately before transfection, the media was replaced with antibiotic free complete DMEM, 10% FBS. The cells were transfected with the sgRNA transfer plasmids (MSCV-U6-sgRNA-IRES-Thy1.1) using TransIT-293 transfection reagent per the manufacturer's protocol (Mirus, Cat# MIR 2700). The following morning, the media was replaced with complete DMEM, 10% FBS, 1% pen/strep. The viral supernatant was collected 48 hours post transfection and filtered through a 0.45 µm, polyethersulfone sterile syringe filter (Whatman, Cat# 6780-2504), to remove cell debris. The viral supernatant was aliquoted and stored until use at -80°C.

Retroviral transduction

Tregs were stimulated as described above for 48-60 hours. Cells were counted and seeded at 3 million cells in 1 mL of media with 2x hIL-2 into each well of a 6 well plate that was coated with 15 µg/mL of RetroNectin (Takara, Cat# T100A) for 3 hours at room temperature and subsequently washed with 1x PBS. Retrovirus was added at a 1:1 v/v ratio (1 mL) and plates were centrifuged for 1 hour at 2000g at 30°C and placed in the incubator at 37°C overnight. The next day, half (1 mL) of the 1:1 retrovirus to media mixture was removed from the plate and 1 mL of fresh retrovirus was added. Plates were immediately centrifuged for 1 hour at 2000g at 30°C. After the second spinfection, cells were pelleted, washed, and cultured in fresh media.

Foxp3 intracellular stain and post-screen cell collection

Tregs were collected from their culture vessels 8 days after the second transduction and centrifuged for 5 min at 300g. Cells were first stained with a viability dye at a 1:1,000 dilution in 1× PBS for 20 min at 4°C, then washed with EasySep Buffer (1× PBS, 2% FBS, 1 mM EDTA). Cells were then resuspended in the appropriate surface staining antibody cocktail and incubated for 30 min at 4°C, then washed with EasySep Buffer. Cells were then fixed, permeabilized, and stained for transcription factors using the Foxp3 Transcription Factor Staining Buffer Set (eBioscience, Cat# 00-5523-00) according to the manufacturer's instructions. Antibodies used in this study are listed in **Table 4**. For the CRISPR screen, Foxp3^{high} and Foxp3^{low} populations were isolated using fluorescence-activated cell sorting by gating on lymphocytes, live cells, CD4⁺ and gating on the highest 40% of Foxp3-expressing cells (Foxp3^{high}) and lowest 40% of Foxp3-expressing cells (Foxp3^{low}) by endogenous Foxp3 intracellular staining. Over 2 million cells were collected for both sorted populations to maintain a library coverage of at least 1,000 cells per sgRNA (1000x).

Isolation of genomic DNA from fixed cells

After cell sorting and collection, genomic DNA (gDNA) was isolated using a protocol specific for fixed cells. Cell pellets were resuspended in cell lysis buffer (0.5% SDS, 50 mM Tris, pH 8, 10 mM EDTA) with 1:25 v/v of 5M NaCl to reverse crosslinking and incubated at 66°C overnight. RNase A (10 mg/mL) was added at 1:50 v/v and incubated at 37°C for 1 hour. Proteinase K (20 mg/mL) was added at 1:50 v/v and incubated at 45°C for 1 hour. Phenol:Chloroform:Isoamyl Alcohol (25:24:1) was added to the sample 1:1 v/v

and transferred to a phase lock gel light tube (QuantaBio, Cat# 2302820), inverted vigorously and centrifuged at 20,000g for 5 mins. The aqueous phase was then transferred to a clean tube and NaAc at 1:10 v/v, 1 µl of GeneElute-LPA (Sigma, Cat# 56575), and isopropanol at 2.5:1 v/v were added. The sample was vortexed, and incubated at -80°C until frozen solid. Then thawed and centrifuged at 20,000g for 30 mins. The cell pellet was washed with 500 µl of 75% EtOH, gently inverted and centrifuged at 20,000g for 5 mins, aspirated, dried, and resuspended in 20 µl TE buffer.

Preparation of genomic DNA for next generation sequencing

Amplification and bar-coding of sgRNAs was performed as previously described⁴⁷ with some modifications. Briefly, after gDNA isolation, sgRNAs were amplified and barcoded with TruSeq Single Indexes using a one-step PCR. TruSeq Adaptor Index 12 (CTTGTA) was used for the *Foxp3*^{low} population and TrueSeq Adaptor Index 14 (AGTTCC) was used for the *Foxp3*^{high} population. Each PCR reaction consisted of 50µL of NEBNext Ultra II Q5 Master Mix (NEB, Cat# M0544), 1µg of gDNA, 2.5µL each of the 10µM forward and reverse primers, and water to 100µL total. The PCR cycling conditions were: 3 minutes at 98°C, followed by 10 seconds at 98°C, 10 seconds at 62°C, 25 seconds at 72°C, for 26 cycles; and a final 2 minute extension at 72°C. After the PCR, the samples were purified using Agencourt AMPure XP SPRI beads (Beckman Coulter, Cat #A63880) per the manufacturer's protocol, quantified using the Qubit ssDNA high sensitivity assay kit (Thermo Fisher Scientific, Cat #Q32854), and then analyzed on the 2100 Bioanalyzer Instrument. Samples were then sequenced on an Illumina MiniSeq using a custom sequencing primer. Primer sequences are listed in **Table 2**.

Pooled CRISPR screen pipeline

Primary Tregs were isolated from the spleen and lymph nodes of three male Foxp3-GFP-Cre/Rosa26-RFP/Cas9 mice aged 5-7 months old, pooled together, and stimulated for 60 hours. Cells were then retrovirally transduced with the sgRNA library and cultured at a density of 1 million cells/ml continually maintaining a library coverage of at least 1,000 cells per sgRNA. Eight days after the second transduction, cells were sorted based on Foxp3 expression defined by intracellular staining. Genomic DNA was harvested from each population and the sgRNA-encoding regions were then amplified by PCR and sequenced on an Illumina MiniSeq using custom sequencing primers. From this data, we quantified the frequencies of cells expressing different sgRNAs in each in each population (Foxp3^{high} and Foxp3^{low}) and quantified the phenotype of the sgRNAs, which we have defined as Foxp3 stabilizing (enriched in Foxp3^{high}) or Foxp3 destabilizing (enriched in Foxp3^{low}).

Analysis of pooled CRISPR screen

Analysis was performed as previously described⁴⁸. To identify hits from the screen, we used the MAGeCK software to quantify and test for guide enrichment⁷. Abundance of guides was first determined by using the MAGeCK “count” module for the raw fastq files. For the targeted libraries, the constant 5’ trim was automatically detected by MAGeCK. To test for robust guide and gene-level enrichment, the MAGeCK “test” module was used with default parameters. This step included median ratio normalization to account for varying read depths. We used the non-targeting control guides to estimate the size factor

for normalization, as well as to build the mean-variance model for null distribution, which was used to find significant guide enrichment. MAGeCK produced guide-level enrichment scores for each direction (i.e. positive and negative) which were then used for alpha-robust rank aggregation (RRA) to obtain gene-level scores. The p-value for each gene was determined by a permutation test, randomizing guide assignments and adjusted for false discovery rates by the Benjamini–Hochberg method. Log2 fold change (LFC) was also calculated for each gene, defined throughout as the median LFC for all guides per gene target. Where indicated, LFC was normalized to have a mean of 0 and standard deviation of 1 to obtain the LFC Z-score. MAGeCK analysis for sgRNA and gene level enrichment and normalized and raw count files can be provided upon request. The top 30 gene level hits for positive regulators of Foxp3 can be found in **Table 1**.

Arrayed Cas9 ribonucleotide protein (RNP) preparation and electroporation

RNPs were produced by complexing a two-component gRNA to Cas9, as previously described²³. In brief, crRNAs and tracrRNAs were chemically synthesized (IDT), and recombinant Cas9-NLS were produced and purified (QB3 Macrolab). Lyophilized RNA was resuspended in Nuclease-free Duplex Buffer (IDT, Cat# 1072570) at a concentration of 160 μ M, and stored in aliquots at -80°C . crRNA and tracrRNA aliquots were thawed, mixed 1:1 by volume, and annealed by incubation at 37°C for 30 min to form an 80 μ M gRNA solution. Recombinant Cas9 was stored at 40 μ M in 20 mM HEPES-KOH, pH 7.5, 150 mM KCl, 10% glycerol, 1 mM DTT, were then mixed 1:1 by volume with the 80 μ M gRNA (2:1 gRNA to Cas9 molar ratio) at 37°C for 15 min to form an RNP at 20 μ M. RNPs were electroporated immediately after complexing. RNPs were electroporated 3 days after initial stimulation. Tregs were collected from their culture vessels and centrifuged for

5 min at 300g, aspirated, and resuspended in the Lonza electroporation buffer P3 using 20 μ l buffer per 200,000 cells. 200,000 Tregs were electroporated per well using a Lonza 4D 96-well electroporation system with pulse code EO148 (mouse) or EH115 (human). Immediately after electroporation, 80 μ L of pre-warmed media was added to each well and the cells were incubated at 37°C for 15 minutes. The cells were then transferred to a round-bottom 96-well tissue culture plate and cultured in either complete DMEM, 10% FBS, 1% pen/strep + 2000U hIL-2 at 200,000 cells/well in 200 μ l of media (mouse) or X-VIVO 15 media (Lonza, Cat# 04-418Q), supplemented with 5% FBS, 50 μ M 2-mercaptoethanol, 10 μ M N-acetyl L-cysteine and 1% pen/strep with hIL-2 at 300U/mL at 200,000 cells/well in 200 μ l of media (human).

PCR amplification of target regions and TIDE analysis

Editing of the DNA was confirmed by Tracking of Indels by DEcomposition (TIDE) analysis 4-8 days post-electroporation and performed as previously described⁴⁹. A total of 5×10^4 to 1×10^5 cells were re-suspended in 30 μ L of QuickExtract DNA Quick Extraction solution (Epicentre) to lyse the cells and extract genomic DNA. The cell lysate was incubated at 65°C for 15 min, 95°C for 5 min, and then stored at -20°C until PCR could be performed across the CRISPR/Cas9 target sites. Unique genomic primers to amplify across the proposed cut sites were designed using the Primer3 online web tool (<http://bioinfo.ut.ee/primer3/>), chemically synthesized (IDT), and suspended at 100 μ M. Each PCR reaction contained 2 μ l 10x High-fidelity PCR buffer (Life Technologies), 3 μ l 2mM dNTPs (Bioline), 0.8 μ l 50mM MgCl₂ (Life Technologies), 0.6 μ l 10 μ M forward primer, 0.6 μ l 10 μ M reverse primer, 0.2 μ l 5U/ μ l Platinum HIFI Taq (Life Technologies), 1 μ l extracted DNA, and 11.8 μ l H₂O. The primer sets used for each crRNA can be found in

Table 3. The thermocycler setting consisted of one step at 95°C for 5 minutes, followed by 14 cycles at 94°C for 20 seconds, 65°C for 20 seconds, and 72°C for 1 minute (wherein the annealing temperature was decreased by 0.5°C per cycle), followed by 35 cycles at 94°C for 20 seconds, 58°C for 20 seconds, and 72°C for 1 minute with one final step at 72°C for 10 minutes. PCR cleanup and capillary sequencing was performed by Quintarabio (San Francisco, CA). Sequencing traces were analyzed with the TIDE webtool (<http://tide.nki.nl/>)⁵⁰.

Isolation, culture and FOXP3 intracellular staining of human Treg cells

Primary human Treg cells for all experiments were sourced from healthy donors from leukoreduction chamber residuals after Trima Apheresis (Vitalant, formerly Blood Centers of the Pacific) or from freshly drawn whole blood under a protocol approved by the UCSF Institutional Review Board (IRB# 13-11950). Peripheral blood mononuclear cells (PBMCs) were isolated from samples by Lymphoprep centrifugation (StemCell, Cat #07861) using SepMate tubes (StemCell, Cat# 85460). CD4⁺ T cells were isolated from PBMCs by magnetic negative selection using the EasySep Human CD4⁺ T Cell Isolation Kit (StemCell, Cat# 17952) and Tregs were then isolated using fluorescence-activated cell sorting by gating on CD4⁺, CD25⁺, CD127^{low} cells. After isolation, cells were stimulated with ImmunoCult Human CD3/CD28/CD2 T Cell Activator (StemCell, Cat# 10970) per the manufacturer's protocol and either electroporated after 48h of stimulation or expanded for 9 days. If expanded, Tregs were restimulated on day 9; 48h before RNP electroporation. Cells were cultured in X-VIVO 15 media (Lonza, Cat# 04-418Q), supplemented with 5% FBS, 50uM 2-mercaptoethanol, 10uM N-acetyl L-cysteine and 1%

pen/strep with hIL-2 at 300U/mL at 1 million cells/mL. For intracellular staining, cells were collected and centrifuged at 300xg for 5mins. Cells were resuspended with a viability dye at a 1:1,000 dilution in 1× PBS for 20 min at 4°C, then washed with EasySep Buffer (1× PBS, 2% FBS, 1 mM EDTA). Cells were then resuspended in the appropriate surface staining antibody cocktail and incubated for 30 min at 4°C, then washed with EasySep Buffer. Cells were then fixed, permeabilized, and stained for transcription factors using the True-Nuclear Transcription Factor Buffer Set (BioLegend, Cat# 424401) according to the manufacturer's instructions. Antibodies used in this study are listed in **Table 4**.

Generation of Usp22 knockout mice

Usp22 floxed mice were generated and used as recently reported⁵¹. The Usp22 target mouse embryonic stem cells from C57BL/6 mice were purchased from the Wellcome Trust Sanger Institute. Blastocyst injections resulted in several chimeric mice with the capacity for germline transmission. Breeding of heterozygous mice yielded *Usp22^{+/+}*, *Usp22^{+/targeted}* but not *Usp22^{targeted/targeted}* mice due to the obligation of Usp22 expression by the neomycin selection and β-gal reporter cassette, which causes embryonic lethality³². We then bred *Usp22^{+/targeted}* mice with Flp recombinase transgenic mice to delete the selection cassette, leading to the generation of *Usp22^{+/fl}* mice, further breeding of which produced *Usp22^{+/+}*, *Usp22^{+/fl}* and *Usp22^{fl/fl}* mice without phenotypic abnormalities in expected Mendelian ratios (**Figs. 6a, 6b**). Treg-specific Usp22-null mice were generated by breeding *Usp22^{fl/fl}* mice with *Foxp3^{YFP-Cre}* mice¹⁷. T cell-specific Usp22-null mice were generated by breeding *Usp22^{fl/fl}* mice with *Lck^{Cre}* mice. Additionally, C57BL/6 Rag-/-mice, SJL CD45.1 congenic mice were purchased from Jackson

Laboratories. These mice were maintained and used at the Northwestern University mouse facility under pathogen-free conditions according to institutional guidelines and using animal study proposals approved by the institutional animal care and use committees. Unless stated otherwise, all figures are representative of experiments with healthy 6-8 week-old mice.

Cell lines, plasmids, antibodies, and reagents

Platinum-E (Plat-E) Retroviral Packaging cells (Cell Biolabs, Inc., Cat# RV-101) were provided by the Bluestone and Cyster Labs and cultured per the manufacturer's instructions. Human embryonic kidney 293 cells (HEK293) were stored in the Fang lab and were cultured in DMEM containing 10% FBS. EG7 lymphoma, MC38 colon cancer, LLC1-OVA lung carcinoma and B16-SIY melanoma cell lines were provided by Dr. Bin Zhang and used for tumor models as previously reported⁵². Cell lines were not genetically authenticated. HEK293 and cancer cell lines were tested for mycoplasma using LookOut Mycoplasma PCR detection kit (Sigma, Cat# MP0035-1KT). Myc-Usp22, Myc-Usp22(C185A), FLAG-Foxp3 and HA-ubiquitin expression plasmids and their tagged vectors were constructed and stored in the Fang lab. Antibodies used for Western blots, Co-IPs and flow cytometry are listed in **Table 4**. PMA (phorbol 12-myristate 13-acetate), ionomycin, and cycloheximide (CHX) were purchased from Sigma. Monesin was from eBioscience.

Cell isolation and flow cytometry for analysis of *Usp22* mice

Peripheral T cells were isolated from mouse spleen by a CD4⁺ T-cell negative (Stem Cell) or positive selection kit (Invitrogen). Enriched CD4⁺ T cells were further sorted for either YFP⁺ (Foxp3⁺) T cells or CD25⁻CD44^{lo}CD62L^{hi} naïve T cells by FACSAria (BD Bioscience). Purity of sorted cells was > 99%. Lymphocytes isolated from the intestinal lamina propria were acquired by following previously described methods⁵³. To isolate tumor-infiltrating lymphocytes, subcutaneous tumors were cut into small fragments and digested by collagenase D (Sigma) and DNase (Sigma) for 1h at room temperature. Flow cytometry was done with a FACSCanto II. Samples were initially incubated with anti-CD16/32 antibodies to block antibody binding to Fc receptor. Single-cell suspensions were stained with relevant antibodies (**Table 4**) and then washed twice with cold PBS containing 3% FBS. For intracellular staining, cells were then fixed, permeabilized, and stained for transcription factors using the Foxp3 Transcription Factor Staining Buffer Set (eBioscience, Cat# 00-5523-00) according to the manufacturer's instructions. For cytokine staining, cells were first stimulated for 4-5 h with 20 ng/ml PMA plus 0.5µM ionomycin in the presence of monesin (10 µg/ml) before staining. Data were analyzed with FlowJo software.

Tumor models

Cultured cancer cells were trypsinized and washed once with PBS. 1x10⁶ tumor cells (for EG7 cells, LLC1 cells and MC38 cells) or 5x10⁴ tumor cells (for B16 melanoma) in suspension were subcutaneously injected into WT or *Usp22^{fl/fl}Foxp3^{YFP-Cre}* 8-10 week-old mice. Tumors were measured every 2-3 days by measuring along 3 orthogonal axes (x,

y, and z) and calculated as $(xyz)/2$ as recently reported⁵². To isolate tumor-infiltrating lymphocytes, tumors were cut into small fragments and digested with 50 mg/ml collagenase D (Sigma) and 20 mg/ml DNase (Sigma) for 1h at room temperature. Tumors were then washed and subsequently strained through a 70 micron filter to achieve single cell suspensions. The tumor size limit agreed by IRB was 2cm³.

***In vitro* Treg suppression assay**

Naïve CD4⁺CD25⁻ T cells (5×10^4) labeled with eFluor 670 cell proliferation dye were used as responder T cells and cultured in 96-well U-bottom plate for 72h together with increasing ratio of sorted YFP⁺ Treg cells from WT or *Usp22^{fl/fl} Foxp3^{YFP-Cre}* mice in the presence of irradiated splenocytes depleted of T cells (5×10^4) plus anti-CD3 (2 µg/ml). The suppressive function of Treg cells was determined by measurement of the proliferation of activated CD4⁺ and CD8⁺ effector T cells on the basis of eFluor 670 cell proliferation dye dilution as reported⁵⁴.

Rescue experiment with Foxp3 overexpression

CD4⁺ cells were isolated from harvested LN and spleens of 8-week-old *Usp22^{+/+} Foxp3^{YFP-Cre}* WT or *Usp22^{fl/fl} Foxp3^{YFP-Cre}* KO mice with the Invitrogen CD4⁺ purification kit (ThermoFisher Cat# 11331D). YFP⁺ Tregs were sorted and subsequently stimulated with 3:1 beads to cells using CD3/CD28 dynabeads in complete DMEM with 2000U hIL-2 at a culture density of ~1 million cells/mL in a 24 well plate for 48 hours. After 48h stimulation, cells were transferred to RetroNectin coated 6-well plates at a density of 3 million cells/mL with a 1:1 ratio of virus to media. RetroNectin coating was done at room temperature for

3hr with 1mL of 15ug/mL in PBS in each of the wells in the 6-well plate. The cells were spininfected for 1hr at 2000xg, then left overnight in the plate at 37°C. The following day, 1mL of new virus was added to the cells for a second spininfection for 1hr at 2000xg. Once spininfection was complete, the cells were plated in a 24-well plate at a density of 1million/well in T cell media in complete RPMI 1640 medium containing 10% FBS, 1% penicillin/streptomycin (MediaTech), 50 μ M β -mercaptoethanol (Gibco), and 1% L-glutamine (Gibco) for 72 hours. After rest, the cells were sorted for YFP⁺GFP⁺ viral infected Tregs. Naïve CD4⁺CD25⁻ T cells (5×10^4) labeled with APC CFSE cell proliferation dye were used as responder T cells and cultured in 96-well u-bottom plate for 72h together with increasing ratio of the sorted GFP⁺YFP⁺ Treg cells with anti-CD3 and anti-CD28 (2 μ g/ml). The suppressive function of Treg cells was assessed by flow cytometry measurement of the proliferation of activated CD4⁺ effector T cells on the basis of APC CFSE cell proliferation dye dilution.

Induced Treg (iTreg) differentiation

0.5×10^6 spenic CD4⁺CD25⁻ naïve T cells were isolated from *Usp22*^{+/+}*Foxp3*^{YFP-Cre} WT or *Usp22*^{fl/fl}*Foxp3*^{YFP-Cre} KO mice and cultured in 24-well plates coated with 3 μ g/ml anti-CD3 and 5 μ g/ml anti-CD28 antibodies for 5 days. For iTreg cell polarization, the cultures were supplemented with IL-2 (5 ng/ml), anti-IFN- γ (2 μ g/ml), anti-IL-4 (2 μ g/ml) and TGF- β (at 2, 5 or 10 ng/ml). Cytokines were purchased from Peprotech.

Th1, Th2 and Th17 *in vitro* differentiations

0.5×10⁶ splenic CD4⁺CD25⁻ naïve T cells were isolated from *Usp22^{fl/fl}Lck^{Cre}* KO or *Usp22^{+/+}Lck^{Cre}* WT mice and cultured in 24-well plates coated with 3 µg/ml anti-CD3 and 5µg/ml anti-CD28 antibodies for 5 days. For skewing towards different T cells subsets, the cultures were supplemented with the following cytokines and antibodies. Th1, IL-2 (5 ng/ml) + IL-12 (5 ng/ml) + anti-IL-4 (1 µg/ml); Th2, IL-2 (5ng/ml) + IL-4 (30 ng/ml); Th17, IL-6 (50 ng/ml) + TGF-β (10 ng/ml) + anti-IFN-γ (1µg/ml)+anti-IL-4 (1µg/ml).

Quantitative PCR (qPCR)

RNA was extracted using a RNeasy Micro Kit (Qiagen, Cat# 74004) from sorted Foxp3⁺ (GFP⁺ or YFP⁺) Tregs and qPCR was performed following the manufacturer's protocol using gene-specific primer sets (**Table 2**).

Histology

Mouse tissues were fixed in 10% formalin and embedded in paraffin. 4µm sections were stained with hematoxylin and eosin. The images were viewed on an olympus CX31 microscope and taken with a PixelLink camera.

Co-Immunoprecipitation and Western blot

Co-IPs and Western blots were performed as previously described⁵⁵. Cells were collected and resuspended in RIPA buffer (Millipore, Cat# 20-188) with protease inhibitors (Roche, Cat# 36363600) and incubated on ice for 30 min. Cells were centrifuged (12000g for 10 min) at 4°C and the cell debris was discarded. The supernatant was incubated with

protein G-sepharose beads at 4°C for 30 min and then with the indicated antibody (1 µg/test) for 2 h followed by incubation with protein G-sepharose beads overnight with rotation at 4°C. The cells were then washed 5 times with RIPA buffer and the protein G-sepharose beads were dissolved with loading buffer and boiled for 5 min. Supernatants were subjected to SDS-PAGE gel and transferred to nitrocellulose membrane. With blocking with 5% (w/v) skim milk in TBS-T buffer, the membrane was incubated overnight with indicated primary antibodies at 4°C followed by HRP-conjugated secondary antibody or with HRP conjugated primary antibodies (**Table 4**). Membranes were then developed with enhanced chemiluminescence (ECL).

Ubiquitination assay

Flag-Foxp3 and HA-ubiquitin plasmids were co-transfected into HEK293 cells using Turbofect Transfection Reagent (Cat# R0532) along with either Myc-empty vector, Myc-Usp22, or the catalytically inactive mutant Myc-Usp22C185A (C>A), where the conserved cysteine (C) residue in the C19 peptidase domain was replaced by an alanine (A) residue. After 48 hours, cells were collected, immunoprecipitated with anti-Flag to pull down Foxp3, and immunoblotted for HA-ubiquitin to assess Foxp3 ubiquitination in the presence or absence of functional Usp22. Whole cell lysate (WCL) controls were immunoblotted with HRP-conjugated Myc and HRP-conjugated Flag to show transfection efficiency.

ChIP-qPCR sample preparation

T cells were polarized using Treg polarizing conditions described above in a 24-well plate for 3 days, and 3 million cells were used per immunoprecipitation. Cells were fixed in 37% formaldehyde for 10 min at 37°C. Glycine was added to a final concentration of 0.125 M, and the incubation was continued for an additional 5 min at room temperature. Cells were washed twice with ice-cold phosphate-buffered saline with 1x Protease Inhibitor cocktail (Roche, Cat# 36363600). Millipore ChIP Assay Kit (Lot 3154126) was used for the remainder of the protocol. Cells were resuspended in 1 ml of SDS lysis buffer (Millipore, Cat# 20-163) with protease inhibitors and set on ice for 15 minutes. Samples were then sonicated at the medium setting (308/608) for 7 minutes. Samples were centrifuged at 14 000 rpm at 4°C for 10 min. After removal of an input control (whole-cell extract), supernatants were diluted 10-fold in ChIP dilution buffer (Millipore, Cat# 20-153), and 1x protease inhibitor. 40 uL of Salmon Sperm DNA/Protein A Agarose-50% (Millipore, Cat #16-157C) for 30 min spinning at 4°C. Agarose pelleted out with brief centrifugation and supernatant moved to a new tube. Samples were incubated with either 4 ul of antibody rabbit anti-IgG (Cell Signaling, Cat# 2729), rabbit anti-USP22 (Abcam, ab195289), ub-Histone H2A Lys119 (Cell Signaling, Cat# 8204S), and ub-Histone H2B Lys120 (Cell Signaling, Cat# 5546P) overnight at 4°C rotation. Samples then incubated with 30 ul of of Salmon Sperm DNA/Protein A Agarose-50% for 1 hour at 4°C with rotation. Agarose was pelleted and placed at rotation for five minutes with Low Salt Immune Complex Wash Buffer (Millipore, Cat #20-154), then pelleted. High Salt Immune Complex Wash Buffer (Millipore, Cat #20-155) was added to the pellet and the sample was spun for five minutes at 4°C then pelleted. The agarose was re-suspended in LiCl Immune Complex Wash

Buffer and placed at rotation for five minutes at 4°C. The samples were then spun down and re-suspended in 1X TE (Millipore, Cat #20-157) and placed at rotation at room temperature for 5 minutes (repeated once more). The sample was then pelleted and resuspended in 100uL of elution buffer (1%SDS, 0.1M NaHCO₃ in water) and placed at rotation for 10 minutes at room temperature. Sample was spun down and supernatant was saved, and step was repeated. 10uL of 5M NaCl was added to the combined eluates and to the input starting material and heated at 65°C overnight. 0.5 M EDTA, 1M Tris-HCl (pH 6.5) and 10mg/mL of protein kinase were added to the samples and incubated at 45°C for one hour. DNA was recovered using a PCR purification kit (Qiagen, Cat #28004).

ChIP-seq sample preparation

Treg cells were collected and either cross-linked in 1% formaldehyde for ten minutes or cross-linked first in 3mM disuccinimidyl glutarate (DSG) in 1X PBS for thirty minutes then in 1% formaldehyde for another ten minutes, both at room temperature. After quenching the excess formaldehyde with a final concentration of 125 mM glycine, the fixed cells were washed in 1X PBS, pelleted, flash-frozen in liquid nitrogen, and stored at -80°C. The cells were thawed on ice and incubated in lysis solution (50 mM HEPES-KOH pH 8, 140 mM NaCl, 1 mM EDTA, 10% glycerol, 0.5% NP40, 0.25% Triton X-100) for ten minutes. The isolated nuclei were washed with wash solution (10 mM Tris-HCl pH 8, 1 mM EDTA, 0.5 mM EGTA, 200 mM NaCl) and shearing buffer (0.1% SDS, 1 mM EDTA, 10 mM Tris-HCl pH 8) then sheared in a Covaris E229 sonicator for ten minutes to generate DNA fragments between ~ 200-1000 base pairs (bp). After clarification of insoluble material by centrifugation, the chromatin was immunoprecipitated overnight at 4°C with antibodies

against Usp22 (1:100 v/v), Rnf20 (1:100 v/v), H2BK120Ub (1:100 v/v), and H2AK119Ub (1:100 v/v). The next day, the antibody bound DNA was incubated with Protein A+G Dynabeads (Invitrogen) in ChIP buffer (50 mM HEPES-KOH pH 7.5, 300 mM NaCl, 1 mM EDTA, 1% Triton X-100, 0.1% DOC, 0.1% SDS), washed and treated with Proteinase K and RNase A. Cross-linking was reversed by incubation at 65°C overnight. Purified ChIP DNA was used for library generation (NuGen Ovation Ultralow Library System V2) according to manufacturer's instructions for subsequent sequencing. ChIP-seq samples were performed with at least 2 biological replicates; with the exception of Usp22 ChIP which has 1 biological replicate with 2 technical replicates (due to poor IP efficiency in the second biological replicate) and H2AK119Ub ChIP performed on Rnf20-RNP cells which has only 1 biological replicate (due to limiting cell number, H2BK120Ub ChIP was prioritized).

ChIP-seq analysis

Single-end 50 base pair (bp) or paired-end 42 bp reads were aligned to mouse genome mm10 using STAR alignment tool (V2.5)⁵⁶. ChIP-seq peaks were called using findPeaks within HOMER using parameters for histone (-style histone) or transcription factor (-style factor) (Christopher Benner, HOMER, <http://homer.ucsd.edu/homer/index.html>, 2018). Peaks were called when enriched > four-fold over input and > four-fold over local tag counts, with Benjamin-Hochberg false discovery rate (FDR) 0.001. For histone ChIP, peaks within a 1000 bp range were stitched together to form regions. ChIP-Seq peaks or regions were annotated by mapping to the nearest TSS using the annotatePeaks.pl command. Differential ChIP peaks were found by merging peaks from control and

experiment groups and called using `getDiffExpression.pl` with fold change ≥ 1.5 or ≤ -1.5 , Poisson p value < 0.0001 . Significance of peak overlap was determined by calculating the number of peaks co-occurring across the entire genome using the HOMER `mergePeaks` program. For the heatmaps of ChIP-seq read densities at sites bound by Foxp3, publicly available Foxp3 ChIP-seq data was used⁴⁰. For enhancer enrichment analysis, we defined the different enhancer classes using publicly available Treg ChIP-seq data for histone modifications H3K4me, H3K4me3, and H3K27ac⁵⁷. All enhancers were called by identifying all H3K4me-positive regions that are at least 1 kb away from the nearest TSS or H3K4me3 mark⁵⁸. These were sub-divided as either active (H3K27ac-positive) or poised (H3K27ac-negative)⁵⁹. To call super enhancers, we used the `findPeaks` program in HOMER with the style option `super`⁵⁸. This was performed with the two H3K27ac ChIP-seq replicates and the sites common between the two were used for further analysis. H2BK120Ub ChIP-seq read density histograms at Treg super enhancers were generated by partitioning each super enhancer into 20 bins and also considering 20 kb upstream and downstream, which were also binned similarly. The number of peaks per kb per bin was calculated and averaged across all super enhancers in the genome. To compare across samples with different number of peaks, the final averaged values were normalized by the number of peaks in each data set. Genome browser tracks for H2BK120Ub ChIP-seq data were generated by combining the tag directories from replicate experiments and using the `makeBigWig` command in HOMER.

RNA sequencing

For RNA-sequencing of *Usp22* KO vs WT Tregs, YFP⁺ cells were sorted from spleen and LN of *Usp22*^{+/+}*Foxp3*^{YFP-Cre} WT or *Usp22*^{fl/fl}*Foxp3*^{YFP-Cre} KO mice (n=5) and total RNA was isolated from 1x10⁶ cells per sample using a RNeasy Mini Kit (Qiagen, Cat# 74104) as previously described⁶⁰. For RNA sequencing of *Usp22* RNP KO and *Rnf20* RNP KO Tregs, GFP⁺ Tregs were sorted from *Foxp3*^{EGFP} mice, stimulated for 48h and electroporated with Cas9 RNPs (n=2). The cells were collected at day 5 post-electroporation and RNA was isolated as described above. ERCC ExFold RNA Spike-In Mixes (Thermo Fisher, Cat# 4456739) were then added to total RNA for each sample. WT and NTC RNP samples were spiked with Mix #1, while KO and RNP KO samples were spiked with Mix# 2. Total RNA was then provided to the Functional Genomics Laboratory at UC Berkeley where RNA-seq libraries were prepared by Oligo dT enrichment followed by a stranded Illumina library prep protocol with the KAPA mRNA HyperPrep kit (Kapa Biosystems, KK8580). Libraries were checked for quality on an AATI Fragment analyzer (Agilent, DNF-935-1000), quantified using the Illumina Quant Universal qPCR Mix (Kapa Biosystems, KK4824), and pooled evenly at 3nM. The Vincent J. Coates Genomics Sequencing Laboratory at UC Berkeley then performed one lane of 150bp paired-end Illumina, HiSeq4000 sequencing followed by demultiplexing and bclfile to fastq conversion using Illumina bcl2fastq v2.19 software (Illumina). Reads were mapped to the GRCm38.p6 assembly (Ensembl annotation) using kallisto v0.45 with default parameters⁶¹. Transcript-level abundance estimates were collapsed to create gene-level count matrices and *Usp22* KO vs WT samples were normalized to the ERCC spike-ins using loess regression⁶². Differentially expressed genes were then detected

using DESeq2 with default parameters⁶³. Pseudogenes beginning with “Gm” were excluded from volcano plots; RNP data was batch corrected and genes with read counts < 10 were removed.

Adoptive transfer model of colitis

Naïve T cells (CD4⁺CD25⁻CD44^{lo}CD62L^{hi}) were sorted from congenic CD45.1 B6.SJL mice and YFP⁺ Treg cells were sorted from WT or *Usp22^{fl/fl}Foxp3^{YFP-Cre}* mice.

Rag1^{-/-} mice were given intraperitoneal injection of naïve T cells (4x10⁵) alone or in combination with WT or *Usp22* KO Treg cells (2x10⁵). After T cell reconstitution, mice were weighed weekly and monitored for clinical signs of disease. Mice were sacrificed when their body weight decreased 20%. At cessation, colons were harvested for measurement and histology and flow cytometry.

Induced experimental autoimmune encephalomyelitis (EAE)

8-10 week-old WT or *Usp22^{fl/fl}Foxp3^{YFP-Cre}* mice were subcutaneously injected with 200µg of MOG₃₃₋₅₅ peptide (Genemed Synthesis). The MOG₃₃₋₅₅ peptide was emulsified in complete Freund's adjuvant (CFA) which contained 200µg of *Mycobacterium tuberculosis* H37Ra (Difco). The mice were then subsequently intraperitoneally injected with 200 ng of pertussis toxin (List Biological Laboratories) on day 0 and day 2. Clinical signs of EAE were assessed daily. Scores were given as follows: 0, no sign of disease; 2, limp tail, 3, hind leg weakness or limp; 3, partial back limb paralysis; 4, complete hind limb paralysis; 5, total limb paralysis.

Data availability

Some data from the screen (Fig. 1) is included as **Table 1** and the remaining screen data and RNA sequencing (Fig. 2, Fig. 8) can be provided upon request. ChIP-seq data that support the findings of this study have been deposited in the Gene Expression Omnibus under the accession code GSE140102 [<https://www.ncbi.nlm.nih.gov/geo/query/acc.cgi?acc=GSE140102>]. Publicly available ChIP-seq and ATAC-seq data were downloaded from the indicated repositories and processed using HOMER v4.8 (Christopher Benner, HOMER, <http://homer.ucsd.edu/homer/index.html>, 2018). Foxp3 ChIP-seq GEO accession code GSE40684; ATAC-seq and ChIP-seq for H3K4me, H3K27ac, H3K4me3 SRA accession number DRP003376.

CHAPTER 4: CONCLUDING REMARKS

Future directions

While this study represents a brute force discovery effort, unfortunately, we were only able to deep dive into the biology of a handful of targets that were identified in our screen. The many remaining hits represent untapped potential of new mechanistic biology that has yet to be revealed.

The future of Treg cell therapies

Several clinical trials have already or are currently exploring ways in which engineered Tregs can be used as a living drug to treat various autoimmune diseases or transplant¹². One critical unmet need for these therapies is to design stable and long-lived Tregs that can prevail in the human body. This study is only the tip of the iceberg in discovering novel targets that can be manipulated to create the potential for stable and effective Treg cell therapies.

REFERENCES

1. Sakaguchi, S., Yamaguchi, T., Nomura, T. & Ono, M. Regulatory T Cells and Immune Tolerance. *Cell* **133**, 775–787 (2008).
2. Zhou, X. *et al.* Instability of the transcription factor Foxp3 leads to the generation of pathogenic memory T cells *in vivo*. *Nature Immunology* **10**, 1000–1007 (2009).
3. Bailey-Bucktrout, S. L. & Bluestone, J. A. Regulatory T cells: stability revisited. *Trends in Immunology* **32**, 301–306 (2011).
4. Overacre-Delgoffe, A. E. & Vignali, D. A. A. Treg Fragility: A Prerequisite for Effective Antitumor Immunity? *Cancer Immunol Res* **6**, 882–887 (2018).
5. Rubtsov, Y. P. *et al.* Stability of the regulatory T cell lineage *in vivo*. *Science* **329**, 1667–1671 (2010).
6. Tanaka, A. & Sakaguchi, S. Regulatory T cells in cancer immunotherapy. *Cell Research* **27**, 109–118 (2017).
7. Maruyama, T., Konkel, J. E., Zamarron, B. F. & Chen, W. The molecular mechanisms of Foxp3 gene regulation. *Semin Immunol* **23**, 418–423 (2011).
8. van Loosdregt, J. *et al.* Stabilization of the Transcription Factor Foxp3 by the Deubiquitinase USP7 Increases Treg-Cell-Suppressive Capacity. *Immunity* **39**, 259–271 (2013).
9. Platt, R. J. *et al.* CRISPR-Cas9 Knockin Mice for Genome Editing and Cancer Modeling. *Cell* **159**, 440–455 (2014).
10. Chen, S. *et al.* Genome-wide CRISPR Screen in a Mouse Model of Tumor Growth and Metastasis. *Cell* **160**, 1246–1260 (2015).

11. Henriksson, J. *et al.* Genome-wide CRISPR Screens in T Helper Cells Reveal Pervasive Crosstalk between Activation and Differentiation. *Cell* **176**, 882–896.e18 (2019).
12. Bluestone, J. A. & Tang, Q. Treg cells—the next frontier of cell therapy. *Science* **362**, 154–155 (2018).
13. Doench, J. G. *et al.* Optimized sgRNA design to maximize activity and minimize off-target effects of CRISPR-Cas9. *Nature Biotechnology* **34**, 184–191 (2016).
14. Li, W. *et al.* MAGeCK enables robust identification of essential genes from genome-scale CRISPR/Cas9 knockout screens. *Genome Biology* **15**, 554 (2014).
15. Beyer, M. & Schultze, J. L. Plasticity of T(reg) cells: is reprogramming of T(reg) cells possible in the presence of FOXP3? *Int. Immunopharmacol.* **11**, 555–560 (2011).
16. Kitoh, A. *et al.* Indispensable role of the Runx1-Cbfbeta transcription complex for in vivo-suppressive function of FoxP3+ regulatory T cells. *Immunity* **31**, 609–620 (2009).
17. Rudra, D. *et al.* Runx-CBF β complexes control Foxp3 expression in regulatory T cells. *Nat Immunol* **10**, 1170–1177 (2009).
18. Ono, M. *et al.* Foxp3 controls regulatory T-cell function by interacting with AML1/Runx1. *Nature* **446**, 685–689 (2007).
19. Yao, Z. *et al.* Nonredundant roles for Stat5a/b in directly regulating Foxp3. *Blood* **109**, 4368–4375 (2007).
20. Williams, L. M. & Rudensky, A. Y. Maintenance of the Foxp3-dependent developmental program in mature regulatory T cells requires continued expression of Foxp3. *Nat. Immunol.* **8**, 277–284 (2007).

21. Beyer, M. *et al.* Repression of SATB1 in regulatory T cells is required for suppressive function and inhibition of effector differentiation. *Nat Immunol* **12**, 898–907 (2011).
22. Koutelou, E., Hirsch, C. L. & Dent, S. Y. R. Multiple faces of the SAGA complex. *Curr Opin Cell Biol* **22**, 374–382 (2010).
23. Schumann, K. *et al.* Generation of knock-in primary human T cells using Cas9 ribonucleoproteins. *PNAS* **112**, 10437–10442 (2015).
24. Rubtsov, Y. P. *et al.* Regulatory T cell-derived interleukin-10 limits inflammation at environmental interfaces. *Immunity* **28**, 546–558 (2008).
25. Martins, M. da S. & Piccirillo, C. A. Functional stability of Foxp3⁺ regulatory T cells. *Trends in Molecular Medicine* **18**, 454–462 (2012).
26. Feng, Y. *et al.* Control of the Inheritance of Regulatory T Cell Identity by a cis Element in the Foxp3 Locus. *Cell* **158**, 749–763 (2014).
27. Li, X., Liang, Y., LeBlanc, M., Benner, C. & Zheng, Y. Function of a Foxp3 cis-Element in Protecting Regulatory T Cell Identity. *Cell* **158**, 734–748 (2014).
28. Zheng, Y. *et al.* Role of conserved non-coding DNA elements in the Foxp3 gene in regulatory T-cell fate. *Nature* **463**, 808–812 (2010).
29. DuPage, M. *et al.* The Chromatin-Modifying Enzyme Ezh2 Is Critical for the Maintenance of Regulatory T Cell Identity after Activation. *Immunity* **42**, 227–238 (2015).
30. Wei, G. *et al.* Global Mapping of H3K4me3 and H3K27me3 Reveals Specificity and Plasticity in Lineage Fate Determination of Differentiating CD4⁺ T Cells. *Immunity* **30**, 155–167 (2009).

31. Josefowicz, S. Z. *et al.* Extrathymically generated regulatory T cells control mucosal T_H2 inflammation. *Nature* **482**, 395–399 (2012).
32. Yu, X. *et al.* SENP3 maintains the stability and function of regulatory T cells via BACH2 deSUMOylation. *Nature Communications* **9**, 3157 (2018).
33. Chen, Z. *et al.* The Ubiquitin Ligase Stub1 Negatively Modulates Regulatory T Cell Suppressive Activity by Promoting Degradation of the Transcription Factor Foxp3. *Immunity* **39**, 272–285 (2013).
34. Dang, E. V. *et al.* Control of TH17/Treg Balance by Hypoxia-Inducible Factor 1. *Cell* **146**, 772–784 (2011).
35. Li, Y. *et al.* USP21 prevents the generation of T-helper-1-like Treg cells. *Nature Communications* **7**, 13559 (2016).
36. Henry, K. W. *et al.* Transcriptional activation via sequential histone H2B ubiquitylation and deubiquitylation, mediated by SAGA-associated Ubp8. *Genes Dev.* **17**, 2648–2663 (2003).
37. Melo-Cardenas, J., Zhang, Y., Zhang, D. D. & Fang, D. Ubiquitin-specific peptidase 22 functions and its involvement in disease. *Oncotarget* **7**, 44848–44856 (2016).
38. Lin, Z. *et al.* USP22 antagonizes p53 transcriptional activation by deubiquitinating Sirt1 to suppress cell apoptosis and is required for mouse embryonic development. *Mol. Cell* **46**, 484–494 (2012).
39. Szklarczyk, D. *et al.* STRING v11: protein-protein association networks with increased coverage, supporting functional discovery in genome-wide experimental datasets. *Nucleic Acids Res.* **47**, D607–D613 (2019).

40. Samstein, R. M. *et al.* Foxp3 Exploits a Pre-Existent Enhancer Landscape for Regulatory T Cell Lineage Specification. *Cell* **151**, 153–166 (2012).
41. Zhou, X. *et al.* Selective miRNA disruption in T reg cells leads to uncontrolled autoimmunity. *The Journal of Experimental Medicine* **205**, 1983 (2008).
42. Luche, H., Weber, O., Nageswara Rao, T., Blum, C. & Fehling, H. J. Faithful activation of an extra-bright red fluorescent protein in ‘knock-in’ Cre-reporter mice ideally suited for lineage tracing studies. *Eur. J. Immunol.* **37**, 43–53 (2007).
43. Bailey-Bucktrout, S. L. *et al.* Self-antigen driven activation induces instability of regulatory T cells during an inflammatory autoimmune response. *Immunity* **39**, 949–962 (2013).
44. Haribhai, D. *et al.* Regulatory T cells dynamically control the primary immune response to foreign antigen. *J. Immunol.* **178**, 2961–2972 (2007).
45. Joung, J. *et al.* Genome-scale CRISPR-Cas9 knockout and transcriptional activation screening. *Nat Protoc* **12**, 828–863 (2017).
46. Stubbington, M. J. *et al.* An atlas of mouse CD4⁺ T cell transcriptomes. *Biology Direct* **10**, 14 (2015).
47. Gilbert, L. A. *et al.* Genome-Scale CRISPR-Mediated Control of Gene Repression and Activation. *Cell* **159**, 647–661 (2014).
48. Shifrut, E. *et al.* Genome-wide CRISPR Screens in Primary Human T Cells Reveal Key Regulators of Immune Function. *Cell* **175**, 1958-1971.e15 (2018).
49. Hultquist, J. F. *et al.* A Cas9 Ribonucleoprotein Platform for Functional Genetic Studies of HIV-Host Interactions in Primary Human T Cells. *Cell Rep* **17**, 1438–1452 (2016).

50. Brinkman, E. K., Chen, T., Amendola, M. & van Steensel, B. Easy quantitative assessment of genome editing by sequence trace decomposition. *Nucleic Acids Res* **42**, e168 (2014).
51. Melo-Cardenas, J. *et al.* USP22 deficiency leads to myeloid leukemia upon oncogenic Kras activation through a PU.1 dependent mechanism. *Blood* blood-2017-10-811760 (2018) doi:10.1182/blood-2017-10-811760.
52. Chen, S. *et al.* Host miR155 Promotes Tumor Growth through a Myeloid-Derived Suppressor Cell–Dependent Mechanism. *Cancer Res* **75**, 519–531 (2015).
53. Qiu, J. *et al.* The Aryl Hydrocarbon Receptor Regulates Gut Immunity through Modulation of Innate Lymphoid Cells. *Immunity* **36**, 92–104 (2012).
54. Lee, S.-M., Gao, B. & Fang, D. FoxP3 maintains Treg unresponsiveness by selectively inhibiting the promoter DNA-binding activity of AP-1. *Blood* **111**, 3599–3606 (2008).
55. Gao, B., Kong, Q., Kemp, K., Zhao, Y.-S. & Fang, D. Analysis of sirtuin 1 expression reveals a molecular explanation of IL-2–mediated reversal of T-cell tolerance. *PNAS* **109**, 899–904 (2012).
56. Dobin, A. *et al.* STAR: ultrafast universal RNA-seq aligner. *Bioinformatics* **29**, 15–21 (2013).
57. Kitagawa, Y. *et al.* Guidance of regulatory T cell development by Satb1-dependent super-enhancer establishment. *Nat. Immunol.* **18**, 173–183 (2017).
58. Whyte, W. A. *et al.* Master Transcription Factors and Mediator Establish Super-Enhancers at Key Cell Identity Genes. *Cell* **153**, 307–319 (2013).

59. Creyghton, M. P. *et al.* Histone H3K27ac separates active from poised enhancers and predicts developmental state. *Proc. Natl. Acad. Sci. U.S.A.* **107**, 21931–21936 (2010).
60. Simeonov, D. R. *et al.* Discovery of stimulation-responsive immune enhancers with CRISPR activation. *Nature* **549**, 111–115 (2017).
61. Bray, N. L., Pimentel, H., Melsted, P. & Pachter, L. Near-optimal probabilistic RNA-seq quantification. *Nature Biotechnology* **34**, 525–527 (2016).
62. Lovén, J. *et al.* Revisiting global gene expression analysis. *Cell* **151**, 476–482 (2012).
63. Love, M. I., Huber, W. & Anders, S. Moderated estimation of fold change and dispersion for RNA-seq data with DESeq2. *Genome Biol* **15**, (2014).

Publishing Agreement

It is the policy of the University to encourage open access and broad distribution of all theses, dissertations, and manuscripts. The Graduate Division will facilitate the distribution of UCSF theses, dissertations, and manuscripts to the UCSF Library for open access and distribution. UCSF will make such theses, dissertations, and manuscripts accessible to the public and will take reasonable steps to preserve these works in perpetuity.

I hereby grant the non-exclusive, perpetual right to The Regents of the University of California to reproduce, publicly display, distribute, preserve, and publish copies of my thesis, dissertation, or manuscript in any form or media, now existing or later derived, including access online for teaching, research, and public service purposes.

DocuSigned by:

F3BCD1174649452... Author Signature

6/12/2020
Date